

# Exploiting Deep Features for Remote Sensing Image Retrieval: A Systematic Investigation

Gui-Song Xia<sup>1</sup>, Xin-Yi Tong<sup>1</sup>, Fan Hu<sup>2</sup>, Yanfei Zhong<sup>1</sup>,  
Mihai Datcu<sup>3</sup>, Liangpei Zhang<sup>1</sup>

<sup>1</sup>*State Key Lab. LIESMARS, Wuhan University, Wuhan 430079, China.*

<sup>2</sup>*School of Electronic Information, Wuhan University, Wuhan 430079, China.*

<sup>3</sup>*German Aerospace Center (DLR), Oberpfaffenhofen, 82234 Weßling, Germany.*

Email: guisong.xia@whu.edu.cn, mihai.datcu@dlr.de, zlp62@whu.edu.cn

November 16, 2021

## Abstract

Remote sensing (RS) image retrieval based on visual content is of great significance for geological information mining. Over the past two decades, a large amount of research on this task has been carried out, which mainly focuses on the following three core issues of image retrieval: visual feature, similarity metric and relevance feedback. Along with the advance of these issues, the technology of RS image retrieval has been developed comparatively mature. However, due to the complexity and multifariousness of high-resolution remote sensing (HRRS) images, there is still room for improvement in the current methods on HRRS data retrieval. In this paper, we analyze the three key aspects of retrieval and provide a comprehensive review on content-based RS image retrieval methods. Furthermore, for the goal to advance the state-of-the-art in HRRS image retrieval, we focus on the visual feature aspect and delve how to use powerful deep representations in this task. We conduct systematic investigation on evaluating factors that may affect the performance of deep features. By optimizing each factor, we acquire remarkable retrieval results on publicly available HRRS datasets. Finally, we explain the experimental phenomenon in detail and draw instructive conclusions according to our analysis. Our work can serve as a guiding role for the research of content-based RS image retrieval.

## 1 Introduction

With the explosive development of earth observation technologies, both the quantity and quality of remote sensing (RS) data are growing at a rapid pace during the past two decades. Several millions of RS images have been delivered by various satellite sensors and stored in massive archives. In order to make full use of RS big data, there is an urgent need of efficient information management, mining and interpretation methods. During the past several decades, significant efforts have been made in developing accurate and efficient retrieval methods to search data of interest from large RS archives.

Primal RS image retrieval systems are queried merely with geographical area, time of acquisition or sensor type [1, 2]. They might be very imprecise and inefficient because text-based image retrieval methods largely rely on manually annotated keywords, which are less relevant to the visual content of RS images. This type of method has restricted the utilization efficiency of RS data, leading to a result that only a fraction of obtained RS data can be fully used.

As content-based image retrieval [3, 4] was proposed in the early 1990s, the efficiency of RS image retrieval has obtained remarkable improvement. New architectures for RS image archives have been constructed, in

which RS images are stored [5] and retrieved [6, 7] based on visual content. So far, several mature RS retrieval systems have come into service [8–17], and satellite data mining technology has been employed in wide practical applications, such as man-made object detection [18, 19], environment monitoring [20], climate monitoring [21], disaster monitoring [22, 23], satellite image time series (SITS) extraction [24] and cross-domain retrieval [25].

Content-based image retrieval indexes with query images, rather than keywords, so its performance is extremely dependent on the visual features of the images. For promoting the accuracy of RS image retrieval, early studies mainly focused on seeking various feature representation methods, hoping to find the best image feature [21, 26–43] or feature combination [44–54].

Nevertheless, due to the drastically increasing volume and complexity of RS data, in some cases visual features may become subjective and ambiguous. Consequently, the simple RS image retrieval systems no longer behave completely satisfactory. To solve this problem, on the one hand, researchers propose to select or design the most suitable similarity metric for specific task [55–58], which can adaptively amend the degree of similarity between image feature vectors. On the other hand, researchers apply relevance feedback to RS retrieval system [14–16, 22, 23, 59–68], aiming to capture the exact query intent of the users and return retrieval results that meet user demand. As described above, visual feature, similarity metric and relevance feedback constitute the three core issues of modern RS image retrieval framework. After years of development, the current RS retrieval methods have been able to solve plenty of practical application problems.

However, for enormous high-resolution remote sensing (HRRS) data, which is of increasingly importance for earth observation, the current methods still have limited capability of recognition and retrieval. One of the key reasons is that it is quite difficult for traditional visual features to represent highly complex geometrical structures and spatial patterns over HRRS images. Considerable amount of literatures has made efforts to extract discriminating features for HRRS image retrieval. The existing retrieval methods can be divided into three types according to the way of feature extracting: methods based on low-level features, methods based on mid-level features and methods based on high-level features. Low-level features are always designed by human on the basis of engineering skills and domain expertise. Diversity low-level features have been exploited in RS retrieval task, mainly including spectral features [26–28, 33, 34], texture features [32, 35, 36, 40–43, 45, 48, 69] and shape features [21, 37, 39, 70]. In contrast, mid-level features can represent more discriminating information by encoding raw features using bag-of-words (BoW) [71], Fisher vector (FV) [72], vector locally aggregated descriptors (VLAD) [73] or their variants. In general, the above hand-craft features have difficulty in accurately describing the semantic information of HRRS data, because the same type of scenes might emerge at different scales, orientations and illuminations at high spatial resolution, causing relevant images of diverse appearance are hard to be retrieved.

To overcome this difficulty, researchers have attempted to take advantage of high-level features derived from Convolutional Neural Networks (CNNs) for HRRS image retrieval. In recent literatures [25, 74, 75], CNN features have proved to be of strong discrimination and able to dramatically improve the HRRS retrieval performance. CNNs are deep hierarchical architectures with parameters (or weights) of each layer learned from large labeled classification datasets, and billions of parameters in pre-trained CNNs can well transfer to relatively small datasets for deep feature extraction. Nevertheless, when CNN models trained for classification are used for domain-specific retrieval, the transferability and adaptability to the target data are uncertain. Various influence factors of transferability are likely to limit the performance of deep feature-based retrieval methods. With this in mind, we intend to further investigate how to use deep features in content-based HRRS image retrieval task.

In this paper, we first analyze the retrieval framework and present a comprehensive review on the three core issues of content-based RS image retrieval: visual feature extraction, similarity metric and relevance feedback, so as to complement existing surveys in literatures [76–79]. Then, we focus on the feature issue and delve into deep features for HRRS image indexing in order to fully advance the task of RS retrieval. We investigate almost all factors concerned to the property of deep features. These factors include the following aspects: CNN architectures, depth of layers, aggregation method for feature maps, dimension of features and fine-tuning. In addition, we propose multi-scale concatenation and multi-patch pooling methods to further

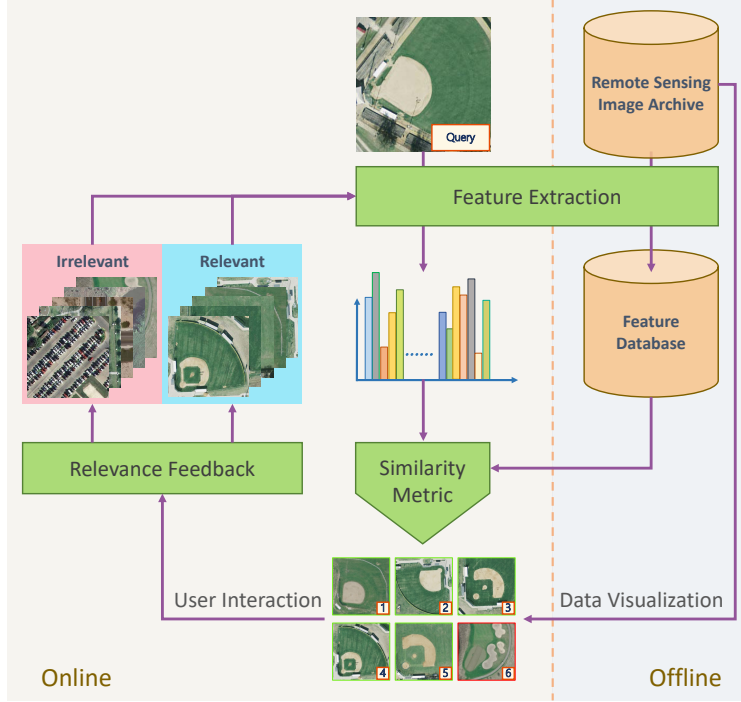


Figure 1: The framework of content-based RS image retrieval system.

enhance the retrieval performance. Finally, we acquire the state-of-the-art results on publicly available HRRS datasets.

In summary, this paper mainly contributes in the following aspects:

- We provide a comprehensive review of content-based image retrieval for RS images, covering the three key issues of retrieval, namely feature extraction, similarity metric and relevance feedback.
- We perform systematic investigation to explore how to utilize deep features for HRRS image retrieval task. We assess almost all potential factors that could influence the performance of deep feature-based retrieval and achieve noteworthy experimental results on three public HRRS datasets.
- We analyze the experimental phenomena in detail, some of which are generalized and some are data-dependent. We draw many instructive conclusions from thorough analysis, which can play a guiding role for domain-specific retrieval tasks. In summary, our work can serve as a useful baseline reference.

## 2 Review on Content-based RS Image Retrieval

In this section, we firstly make a detailed introduction to content-based RS image retrieval, and then comprehensively review the existing research works in this field. We take three key aspects consisting of feature extraction, similarity metric as well as relevance feedback into consideration and analyze their functions for retrieval task.

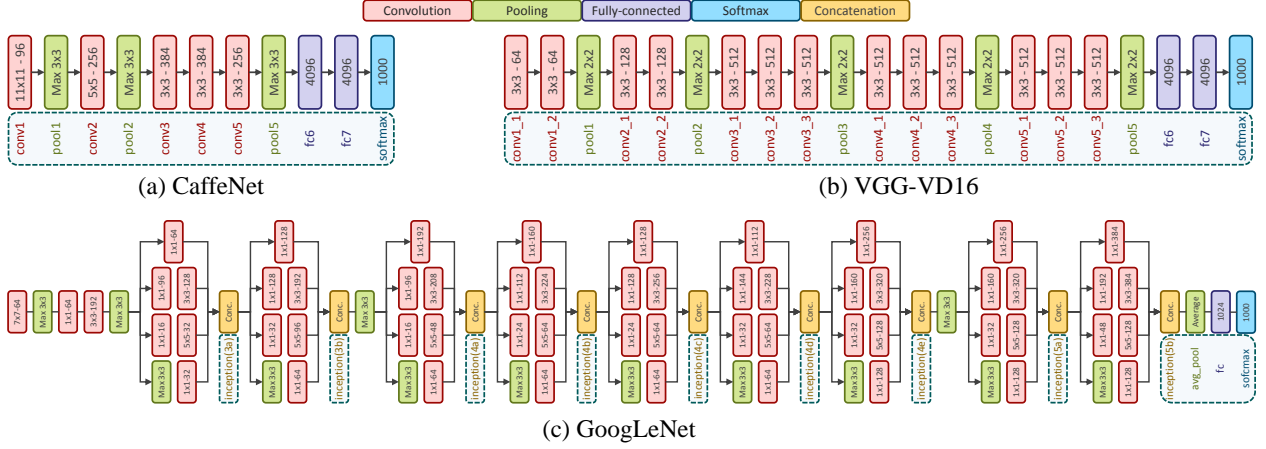


Figure 2: Simplified architecture diagram of three representative CNN models: CaffeNet, VGG-VD16 and GoogLeNet.

## 2.1 An Overview of RS Image Retrieval

The goal of content-based RS image retrieval is to find a set of images generally acquired from the regions of similar land-cover types, which contain the information desired by the users, from RS archives. We indicate the images stored in database to be retrieved as reference images. If the retrieval system returns reference images containing relevant visual content to a given query image, we regard them as correct retrieval results.

A content-based image retrieval framework at least consists of two stages. The first stage extracts image features for representing the physical object and scene from both the input query image and reference images. The second stage calculates the visual similarity between the query image and each reference image with feature vectors and then returns a ranked list of relevant images ordered by the degree of similarity. Moreover, if visual features and similarity metrics have limited ability to accurately measure the relationship between image contents, after obtaining the initial results, relevance feedback can interactively revise the retrieval ranking in iterations. The overall framework of a RS image retrieval system is illustrated in Fig. 1.

RS images are composed of unstructured arrays of pixels, from which visual features need to be extracted for semantic content understanding. Because similar scenes might present various complex structures and textures in RS images, only sufficiently discriminating features can effectively determine whether they are relevant. Hence appropriate feature representations can significantly improve the performance of retrieval.

Similarity metrics study the distance between feature vectors, thereby the similar degree between image contents is able to be measured. For particular retrieval task, a suitable similarity metric can make the results to be more desirable.

Relevance feedback automatically adjusts the retrieval results to meet user demand based on user feedback of the previous ranking. It means that the researchers do not need to specify superior visual feature or similarity metric for better retrieval performance, but only need to point out whether indexed images are similar to the query or not. This technology can capture the information actually needed by users and is of great significance for the practical applications of RS retrieval systems.

In order to gain an insight into content-based image retrieval of RS imagery, we present a comprehensive review on this task focusing on the above three core issues. Though there has been a few surveys on broad content-based RS image retrieval research [76–79], they particularly give attention to certain sections of RS data mining. Our work can serve as a thorough complement for the previous surveys.

## 2.2 How to Represent RS Images

RS image retrieval methods can be divided into three categories based on the way of feature extraction: methods based on low-level features, methods based on mid-level features and methods based on high-level features. We introduce the relative literatures at length in the following.

### 2.2.1 Methods based on low-level features

Visual content can be typically defined by a set of hand-crafted features extracted which describe the spectral, texture or shape information of RS images.

Spectral features are one of the simplest features, yet they describe the most prominent different information from natural images [80]. Spectral features have been used in many research works [26–28, 33, 34]. They encode the reflectance of the corresponding areas of the Earth's surface, which results in serious sensitivity to noise and illumination change.

Texture features are generally understood as ordered structures composed of a group of pixels. A number of important texture features have been proposed, such as gray level co-occurrence matrices (GLCM) [81], wavelets [82, 83], Gabor filters [84, 85] and local binary patterns (LBP) [86]. Texture representations are widely applied to RS image retrieval in the form of single feature [32, 35, 36, 40–43] or combination of multiple features [45, 48, 69]. For instance, Li *et al.* [45] combine gray level difference features, circular Moran autocorrelation functions, Robert Gradient, co-occurrence matrix based features, measures of fractal dimension coupled with first- and second-order moments [87–89] to retrieve RS images provided by various satellite instruments. Erchan Aptoula [69] makes use of the circular covariance histogram (CCH) and the rotation-invariant point triplets (RITs) [90, 91], as well as develops two new texture features relying on the Fourier power spectrum (FPS) of a multiscale quasi-flat-zone (QFZ). Texture features are more robust to illumination variations and take less computation, thus they perform desirably for RS retrieval task.

Shape features are important cue for identification and recognition surface objects in RS images [21, 37, 39, 70]. Ma *et al.* [37] retrieve infrared images with similar polygons derived from association spaces. Scott *et al.* [70] employ a bitmap shape representation that provides a small fixed encoding size.

Other types of features are also developed for RS image retrieval. Newsam *et al.* [38] investigate how scale-invariant feature transform (SIFT) [92] extracted from interest points compared to global texture features for similarity retrieval. Xia *et al.* [93–95] develop structural features from the shape ensembles and their relationships relying on topographic maps [96] and shape-based image indexing scheme [97].

In some cases, single type of low-level features lacks discrimination, therefore, researchers explore combinations of diverse types of features to improve the retrieval results [10–13, 44, 46, 47, 49–54, 98]. Particularly, in [49], spectral features and texture features are fused, including the color histograms [99], the wavelet-based textures and the grey level difference textures [100]. Tobin *et al.* [10, 11] construct a large-scale geospatial indexing system, which characterizes image texture and structure respectively using LBP and local edge patterns (LEP) [101] compressed by linear discriminant analysis [102]. Shyu *et al.* [12, 13] develop a framework for geospatial information retrieval and indexing system (GeoIRIS), they use features comprised of the spectral histograms, GLCM, as well as shape features generated from linear structures [103] and differential morphological profiles (DMP) [104]. Inspired by [105, 106], Maheswary *et al.* [50] employ spectral features and texture features that are grouped based on particular threshold value. In [51], Samal *et al.* represent RS images with combined features consisting of spectral and spatial attributes, which are extracted by spatial autocorrelation measures [107, 108], at different resolution levels.

### 2.2.2 Methods based on mid-level features

In contrast with low-level features, mid-level features embed raw descriptors into representative visual vocabulary space and encode feature spatial distribution to capture semantic concepts of RS images. Mid-level features are more invariant to differences in appearance caused by changes of scale, rotation or illumination, and they can better represent the complex image textures and structures with more compact feature vectors.

The general pipeline to extract mid-level features is firstly obtaining local image descriptors, such as spectral, texture or local invariant features, and then aggregating them into holistic representations using encode methods, e.g., BoW, FV, and VLAD.

BoW is a widely used basic encoding method, it employs k-means clustering to construct visual codebook and counts local features into the histogram of codebook. Concretely, Yang and Newsam [109] exploit BoW to encode both saliency- and grid-based SIFT features to index HRRS images. Erchan Aptoula [110] extracts morphological texture descriptors, i.e., CCH and RITs, from local sub-windows and transforms them to mid-level features with BoW. Their studies have shown the effectiveness of encoded features compared with local low-level features. Besides, in order to improve the retrieval performance of the typical BoW framework, Yang *et al.* [111] propose to generate codebook with local features derived from sample images instead of the cluster method.

VLAD is an advanced version of BoW, apart from feature distribution, it additionally counts the distance between local features and cluster centers. In [112], Bosilj *et al.* utilize VLAD to encode local pattern spectra [113] calculated from pyramid grids and obtain high-precision retrieval results on HRRS images. Ozkan *et al.* [114] study the performance of BoW, VLAD and product quantized VLAD (VLAD-PQ) [115] on SIFT feature. The results demonstrate that BoW behaves better in calculation speed while VLAD behaves better in indexing accuracy.

Multi-scale spatial information has also been exploited in feature encoding. Wang *et al.* [116] combine two types of low-level features to be encoded: holistic GIST [117] and local SIFT, and encode them via spatial pyramid matching based on sparse codes (ScSPM) [118]. The fusion of holistic and local features enhances the discrimination of mid-level features.

Except for the above encoding methods, there are other unsupervised feature learning methods have been utilized to construct features with higher level of semantic information. In [119], Zhou *et al.* use auto-encoder to produce sparse representations from SIFT features. And Li *et al.* [120] design hierarchical neural networks with different layers to learning unsupervised features from different scales, which can represent complex structure information in HRRS images.

### 2.2.3 Methods based on high-level features

The principal theory of CNNs had been mature in the 1990s [121], but they were not highly regarded until Krizhevsky et al. [122] showing remarkable image classification results on the ImageNet Large Scale Visual Recognition Challenge (ILSVRC) [123] in 2012, and up to this day, CNNs have attained surprising dominance in computer vision research area.

The multistage architecture of CNN models can simulate very complex nonlinear functions and automatically learning parameters during the training process. Therefore, CNN models are able to capture the essential characteristics of training data so as to represent discriminating visual features for images. Deep features extracted from CNN models contain high-level semantic information and have proved to be prominent in solving various visual problems, such as image classification, object detection, fine-grained recognition, and image instance retrieval.

There are several approach to retrieve basing on CNNs, including obtaining features by existing CNNs from convolutional (conv.) layers [124–127] or fully-connected (FC) layers [128–130], fine-tuning off-the-shelf CNN models with domain-relevant datasets as feature extractors [129], or developing tailored CNN architectures for specific retrieval task [131], etc.

There is a small amount of research works that use high-level features for RS retrieval up till now. In [75], Napoletano compares retrieval performance of high-level features derived from off-the-shelf CNN models with mid-level features, including SIFT features encoded by BoW, VLAD, Fisher vector (FV) [72] and LBP encoded by BoW, on several HRRS datasets. The CNN models used to extract FC features in this literature are AlexNet [122], Caffe reference model (CaffeRef) [132], VGG networks [133], and VGG-VD networks [134]. They show much higher retrieval accuracy than mid-level features on all HRRS dataset.

Except for off-the-shelf CNN models originally trained on ImageNet dataset, Zhou *et al.* [74] construct

a novel CNN architecture named as low dimensional CNN (LDCNN), which is based on conventional conv. layers and a three-layer perception, for HRRS image retrieval task. In the architecture of LDCNN, mlpconv layers [135] are added behind the last conv. layer and the conventional FC layers are replaced with global average pooling layers. LDCNN is trained by a large-scale benchmark dataset: aerial Image data set (AID) [136], hence it has greater bias towards HRRS data. It provides comparable retrieval performance compared with off-the-shelf CNN models on different HRRS datasets.

Deep features are also used to solve the complicated cross-domain problems because of their strong generalization ability. Jiang *et al.* [25] firstly put forward sketch-based RS image retrieval problem and propose a multi-scale deep model to bridge the gap between abstract expression and real RS images.

Nevertheless, there is still no a comprehensive investigation for content-based image retrieval of HRRS images. Furthermore, we don't know if the developed research conclusions of natural image retrieval are transferable to RS image retrieval, since the diversity of data has some degree of impact on index results. To sum up, it is not clear how to maximize the performance of high-level feature-based HRRS image retrieval yet.

### 2.3 How to Measure Feature Similarity

Similarity metric (or distance function) is a function that defines the distance between visual feature vectors, which is the basis of pattern recognition. For it is one of the core issues in content-based image retrieval, similarity metric is of great research significance.

For the same retrieval task, different similarity metric may lead to different ranking results. Bao *et al.* [55] experimentally investigate eight similarity metrics through RS image retrieval and demonstrate the impact of them. Similarity metrics examined in this work can be divided into two major categories: general feature vector based metrics, including Euclidean distance, city-block distance, dominance distance and cosine of the angle, and histogram vector based measures, including histogram intersection, center moment,  $\chi^2$  statistical distance and Bhattacharyya distance. This research work intuitively demonstrates the importance of similarity metrics for content-based RS retrieval task.

Apart from selecting the appropriate similarity metrics, distance functions also can be manually constructed for specific retrieval task in order to deal with the similarity between a wide variety of visual features. For instance, in [56], an informational similarity metric is introduced for compressed RS data mining. In [57], a hyper-spectral image distance based on endmember induction algorithms (EIAs) [137] is developed. This similarity metric serves as a function of the distances between individual image endmembers and provides remarkable retrieval performance on hyper-spectral images. In [58], dictionary-based similarity metrics are employed for retrieval on different hyper-spectral image datasets. Three similarity metrics are compared, including the normalized dictionary distance (NDD) [138], the fast dictionary distance (FDD) [139] and the normalized compression distance NCD [140]. Experimental results of this literature validate the applicability of dictionary-based similarity metrics for hyperspectral image retrieval.

However, manually constructing a similarity metric may be inefficiency and not robust to different data source, metric learning can be an ideal alternative. In contrast to handcrafted similarity metrics, metric learning is capable of automatically learning distance function for a specific retrieval task according to task requirement. For calculating the distance of images, its function is learning how to maximize the inter-class variations and minimize the intra-class variations from training samples.

Metric learning has very wide applications in content-based image retrieval [141–144]. Unsupervised metric learning has been successfully applied to RS retrieval, for example, [145] models RS images with graphs and uses an unsupervised graph-theoretic method to measure the similarity between the query graph and the graphs of images in the archive. This matching strategy significantly improves the retrieval performance on HRRS images.

In particular, for natural images, deep learning-based metric learning method has obtained the development in recent years and boosted the efficiency of weakly supervised retrieval problem. Nevertheless, there has been little research on applying it to RS images yet. In [146], geographic coordinates are seen as weakly

supervised information and used to train a triplet network for street view image retrieval. This novel work utilizes VLAD to encode feature maps of off-the-shelf CNN models, in which the cluster centroids are learned by metric learning.

## 2.4 How to Optimize Ranking Result

Due to the huge amount and the rapid growth of RS data, even when the visual features are discriminating and the similarity metric is adaptive, the ranking results of content-based RS image retrieval may still not be very satisfying. Therefore, intelligent feedback techniques become essential for efficiently and effectively retrieving required images from massive RS archives.

Relevance feedback can iteratively adjust the retrieval results according to the previous ranking, thereby optimizing the results for the target retrieval tasks. Once the ranking of the initial retrieval is returned, there are two ways to select a subset of relevant images: automatically selection and manually selection, which are applied to pseudo relevance feedback and explicit relevance feedback respectively. No matter how the relevant images are selected, relevance feedback can better capture the needed image information in the iterative process.

For pseudo relevance feedback [147], the top several returned results are regarded as relevant images, and their features are used for query expansion. Concretely, Wang *et al.* [116] develop a three-layer framework that combines the advantage of query expansion and feature fusion. The top six retrieved images in each iteration are evaluated for generating positive and negative data, and simple multiple kernel learning (SimpleMKL) [148] is exploited to learn suitable query-dependent fusion weights so as to expand the query.

In contrast, for explicit relevance feedback [147], it is the users that manually mark retrieved images as relevant or irrelevant at every feedback round. There are three different methods to re-estimate the target query using relevancy labels, namely query-point movement and re-weighting method [149, 150], probability distribution-based method [151, 152] and machine learning-based method [153, 154].

The idea of query-point movement and re-weighting method is to adjust the query point in the feature space according to the users feedback information, making it closer to the ideal query point, and then use the adjusted query point to re-calculate the retrieval ranking. For example, [22] updates the query vector weights based on the user rankings in each feedback iteration.

The process of probability distribution-based method can be seen as equivalent to minimizing the probability of retrieving irrelevant images. In other words, it is based on Bayesian inference method. Specifically, assume there is a mapping from the visual features to the image categories, and the purpose of probability distribution-based relevance feedback is to find the optimal mapping that can reduce the probability of retrieval error to minimum [7, 14, 23, 59, 62]. In particular, [7] constructs an intelligent satellite information mining system, which captures spatial information of RS images with Bayesian inference method [30, 31]. In [59], interactive learning is used to develop a probabilistic retrieval scheme, and a very intuitive user interface is built for providing instantaneous feedback. Datcu *et al.* [14–16] develop a knowledge-driven information mining system that extracts RS image features offline and define user-specific semantic image content label online. This system can satisfy various user needs and application requirements.

Machine learning-based relevance feedback can be considered as a binary-classification problem: the relevant retrieved images are positives while the irrelevant retrieved images are negatives. Hence the typical supervised machine learning method can be applied to content-based image retrieval by training the classifier with the manually annotated images of two classes. Machine learning-based relevance feedback returns image ranking according to the category scores derived from the classification model. In each iteration of feedback, the classifier can be trained with the feedback samples of the current round, or with the combination of the current and the former feedback samples via incremental learning. Commonly used classifiers include decision tree [63, 68], Bayesian networks [66], support vector machine (SVM) [60, 61, 64, 65] and so on.

Specifically, Ferecatu and Boujemaa [60] utilize SVM to optimize the information transfer between the user and the retrieval system, showing that relevance feedback can provide significant performance improvement to RS image retrieval. Demir and Bruzzone [61] present a SVM classifier-based active learning method to

find the most informative images from RS archives for reducing the annotation effort. This novel retrieval framework is proven to generate efficient retrieval performance requiring less relevance feedback iterations as well as less annotation effort.

In relevant feedback, users usually give binary labels on returned images: similar or not similar. But in practical, RS image rarely contain only one visual content, therefore, general interactive learning may result in suboptimal model. To overcome this problem, Barb and Shyu [67] introduce graded relevance feedback to RS image retrieval. In this work, users mark returned images with graded ratings, and so more precise reranking results can be obtained.

Apart from the above three core issues which are closely related to the retrieval performance, there are also many literatures aiming at improving the retrieval computational efficiency in the RS community, including taking advantages of distributed computation [155], tree structures [10–13, 51, 70] and hash codes [37, 156–159]. The partition-tree can recursively divide the stored data into subspaces and then organize the subspaces with tree structures, such as the  $k$ -dimensional (KD) tree, the entropy balanced statistical (EBS) KD tree, the entropy balanced bitmap (EBB) tree and the quad tree. The hashing can map high-dimensional image feature vectors into compact binary hash codes, which constitute a hash table that reduces the time and memory required for accurate retrieval.

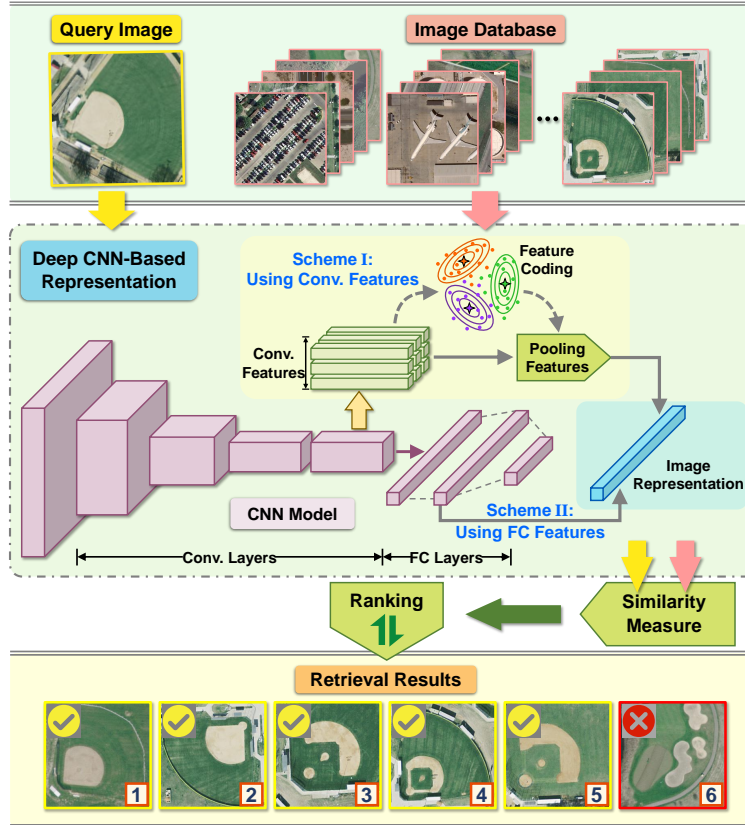


Figure 3: The pipelines of scheme (I) and scheme (II) for deep CNN feature extraction as well as image retrieval.

### 3 Deep Features for RS Image Retrieval

Even though some literatures have made advantages of deep features for RS retrieval task, there still no comprehensive research on how to optimize the transferability of CNN models to RS retrieval. With this in mind, we investigate almost all variables concerned to property of CNN representations on multiple public HRRS datasets and analyze the effects of each factor with retrieval results.

In this section, we present the methods to extract deep features for HRRS image retrieval. An elementary content-based image retrieval framework is composed of two stages, for an image dataset which contains  $N$  images, the first stage extracts the visual features  $\mathbf{f}^q$  and  $\mathbf{f}^r$  respectively from the query image  $\mathbf{I}^q$  and all the reference images  $\mathbf{I}^r$ , for  $r = 1, \dots, N$ . The second stage calculates the distances  $D_{qr} = d(\mathbf{f}^q, \mathbf{f}^r)$  between extracted feature vectors and then ranks retrieved images according to the values of  $D_{qr}$ , i.e., the more similar  $\mathbf{f}^q$  and  $\mathbf{f}^r$  are, the lower  $\mathbf{I}^r$  ranks. Where  $d(\cdot, \cdot)$  stands for a distance function, we consider Euclidean, Cosine, Manhattan and  $\chi^2$ -square distance metrics in our experiments.

Because conv. and FC features derived from different depths in CNN architecture, they are at various representation levels. Conv. features correspond to local responses of every image region, while FC features contain global information of the holistic image, this diversity may lead to different impact on different data. We are not sure which type of deep feature is more adaptive for RS image retrieval.

Another problem is that image retrieval is unlike image classification, there is no labeled training data for every category available. Consequently, the off-the-shelf CNN models may have limited capability of transferring for RS image data to produce discriminating representations. This defect is likely to hold back the performance of HRRS image retrieval.

On account of the aforementioned considerations, we make use of five representative CNN models: CaffeNet [132], VGG-M [133], VGG-VD16, VGG-VD19 [134], GoogLeNet [160], and utilize thorough approaches for feature extraction. The architecture of CaffeNet, VGG-VD16 and GoogLeNet are particularly demonstrated in Fig. 2.

And we mainly conduct three schemes on the foundation of CNNs to obtain HRRS image descriptors: respectively adopting deep features derived from conv. and FC layers of pre-trained CNNs for effectiveness comparison, the process of which is illustrated in Fig. 3; and performing fine-tuning strategy on several off-the-shelf CNN models for targeted feature extraction, demonstrated in Fig. 4.

#### 3.1 Scheme (I): Employing Conv. Features

The activations of intermediate conv. layers reflect relatively low-level features because of insufficient feature learning from the training data, thus conv. activations tend to catch finer grained information that may be beneficial to content-based retrieval.

When passing an image  $\mathbf{I}$  through a CNN, the outputs from conv. layers are feature maps, each element in which corresponds to a receptive field of the input image. Suppose the responses of a certain conv. layer form  $L$  feature maps and the size of each feature map is  $W \times H$ , the activations of examined layer can be interpreted as  $W \times H$   $L$ -dimensional vectors that describe local features for  $\mathbf{I}$ , where the channel number  $L$  depends on the inherent structure of CNN, and the feature map spatial resolution  $W \times H$  rests with the architecture of CNN, the adopted layer and the size of image  $\mathbf{I}$ .

Feature maps cannot be straightforwardly used as image descriptors for retrieval, consequently they are normally aggregated into compact global descriptors by aggregation methods. We denote the activation at the spatial coordinates  $(x, y)$  of the  $z$ -th feature map as  $a_{x,y}^z$ , for  $x = 1, \dots, W$ ,  $y = 1, \dots, H$ ,  $z = 1, \dots, L$ , and indicate the global feature vector of the input image  $\mathbf{I}$  as  $\mathbf{f}$ . We apply several promising aggregation strategies, which can be divided into pooling and encoding methods.

##### 3.1.1 Pooling Methods

Here we introduce five pooling methods for conv. feature aggregation: max pooling, mean pooling, hybrid pooling [125], sum-pooled convolutional features (SPoC) [126], and cross-dimensional weighting and pooling

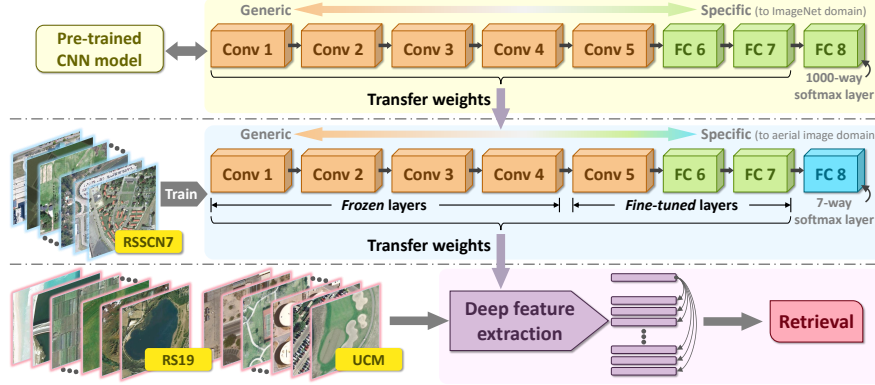


Figure 4: Overview of fine-tuning for scheme (III).

features (CroW) [127]. When dealing with feature maps using pooling methods, we treat conv. activations as  $L$  two-dimensional matrices and each of them composed of  $W \times H$  elements:  $a_{1,1}^z, a_{1,2}^z, \dots, a_{W,H}^z$ .

- *Max Pooling*: Max pooling generates  $L$ -dimensional feature vector  $\mathbf{f} = [f_1, \dots, f_z, \dots, f_L] \in \mathbb{R}^L$ , where every element in resulting representation is simply the max activation of a corresponding feature map:

$$f_z = \max_{1 \leq x \leq W, 1 \leq y \leq H} a_{x,y}^z. \quad (1)$$

- *Mean Pooling*: Analogous, the  $L$ -dimensional output  $\mathbf{f} = [f_1, \dots, f_z, \dots, f_L] \in \mathbb{R}^L$  of mean pooling is a set of average values yielded from corresponding feature maps:

$$f_z = \frac{\sum_{y=1}^H \sum_{x=1}^W a_{x,y}^z}{WH}. \quad (2)$$

- *Hybrid Pooling*: The feature vector produced by hybrid pooling is the intuitional concatenation of max pooling and mean pooling representations, therefore the hybrid pooling representation is with a dimension of  $2L$ .
- *SPoC*: SPoC representation  $\mathbf{f} = [f_1, \dots, f_z, \dots, f_L] \in \mathbb{R}^L$  is acquired with center-prior Gaussian weighting on spatial of feature maps followed by sum pooling:

$$f_z = \sum_{y=1}^H \sum_{x=1}^W g_{(x,y)} a_{x,y}^z. \quad (3)$$

The function  $g_{(x,y)}$  is constructed based on Gaussian weighting scheme:

$$g_{(x,y)} = \exp \left\{ - \frac{(y - \frac{H}{2})^2 + (x - \frac{W}{2})^2}{2\sigma^2} \right\}, \quad (4)$$

where  $\sigma$  is set to be  $1/3$  of the distance between the center and the closest boundary of the input image.

- *CroW*: CroW is a promotion version of SPoC with specific non-parametric schemes for both spatial and channel wise weighting. Firstly, activations with positive values of each feature map channel are counted as:

$$\phi^z = \frac{\sum_{y=1}^H \sum_{x=1}^W \theta_{x,y}^z}{WH}, \quad (5)$$



Figure 5: Sample images from each category in the RS19 dataset are shown.

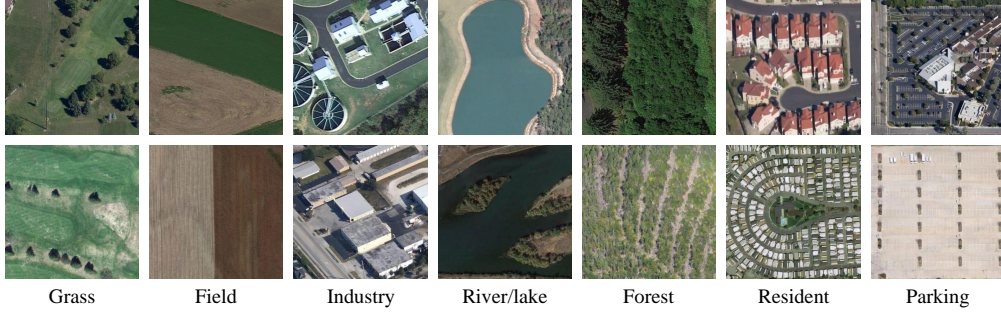


Figure 6: Sample images from each category in the RSSCN7 dataset are shown.

where  $\theta_{x,y}^z = 1$  if  $a_{x,y}^z > 0$ , and  $\theta_{x,y}^z = 0$  if  $a_{x,y}^z \leq 0$ . The spatial weighting  $\alpha_{x,y}$  and channel weighting  $\beta^z$  are defined as follows:

$$\alpha_{x,y} = \frac{\sum_{z=1}^L a_{x,y}^z}{(\sum_{y=1}^H \sum_{x=1}^W (\sum_{z=1}^L a_{x,y}^z)^2)^{\frac{1}{2}}}, \quad (6)$$

$$\beta^z = \begin{cases} \log(\sum_{z=1}^L \phi^z / \phi^z) & \phi^z > 0 \\ 0 & \phi^z = 0. \end{cases}$$

thereby the final feature  $\mathbf{f} = [f_1, \dots, f_z, \dots, f_L] \in \mathbb{R}^L$  is obtained by weight-summing:

$$f_z = \sum_{y=1}^H \sum_{x=1}^W \alpha_{x,y} \beta^z a_{x,y}^z. \quad (7)$$

### 3.1.2 Encoding Methods

Here we introduce three traditional encoding methods for aggregating feature maps into holistic feature vectors: bag-of-words (BoW) [71], improved Fisher kernel (IFK) [161] and vector locally aggregated descriptors



Figure 7: Sample images from each category in the UCM dataset are shown.

(VLAD) [73]. When processing feature maps with encoding methods, we interpret conv. activations as  $W \times H$  feature vectors:  $\{v_{1,1}, v_{1,2}, \dots, v_{x,y}, \dots, v_{W,H}\}$ , here  $v_{x,y} = [a_{x,y}^1, \dots, a_{x,y}^L] \in \mathbb{R}^L$ .

- *BoW*: BoW describe image information with statistics on the spatial distribution of local feature vectors. A codebook of  $k$  centroids  $\{c_1, \dots, c_i, \dots, c_k\} \in \mathbb{R}^{L \times k}$ , for  $i = 1, \dots, k$ , is learned from local feature set  $\{v_{1,1}, v_{1,2}, \dots, v_{W,H}\}$  via k-means clustering, then every local feature is assigned to its closest centroid. The output of BoW is a  $k$ -dimensional vector  $\mathbf{f} = [f_1, \dots, f_i, \dots, f_k] \in \mathbb{R}^k$ , where  $f_i$  denotes the amount of local features that is assigned to  $c_i$ .
- *IFK*: IFK is a combination of generative and discriminative approaches, it utilizes Gaussian mixture model (GMM) with  $k$  Gaussian components to construct a probability density distribution of local features. Parameters of GMM is denoted as  $\lambda = \{\omega_i, \mu_i, \Sigma_i\}, i = 1, \dots, k$ , where  $\omega_i$ ,  $\mu_i$  and  $\Sigma_i$  are respectively the mixture weight, mean vector and covariance matrix of Gaussian distributions. Then the  $L$ -dimensional gradient vectors  $\mathcal{G}_{\mu,i}$  and  $\mathcal{G}_{\Sigma,i}$ , which are separately with respect to the mean vector and covariance matrix of  $i$ -th Gaussian component, are derived based on the feature set  $\{v_{1,1}, v_{1,2}, \dots, v_{W,H}\}$ . The final IFK representation is a  $2L \times k$ -dimensional vector indicated as  $\mathbf{f} = [\mathcal{G}_{\mu,1}, \mathcal{G}_{\Sigma,1}, \dots, \mathcal{G}_{\mu,k}, \mathcal{G}_{\Sigma,k}] \in \mathbb{R}^{2L \times k}$ .
- *VLAD*: VLAD is similar to BoW, yet it considers the statistical distribution of local features as well as the vector difference between local features and centroids simultaneously. The set of feature vectors  $\{v_{1,1}, v_{1,2}, \dots, v_{x,y}, \dots, v_{W,H}\}$  is clustered into a codebook  $\{c_1, \dots, c_i, \dots, c_k\} \in \mathbb{R}^{L \times k}$  of  $k$  visual words with k-means, where  $i = 1, \dots, k$ . A local feature  $v_{x,y}$  is assigned to its nearest visual word  $c_i = NN(v_{x,y})$  and the vector difference  $v_{x,y} - c_i$  between them is recorded and accumulated, ultimately, a VLAD descriptor with a dimension of  $L \times k$  is represented as  $\mathbf{f} = [\sum_{NN(v_{x,y})=c_1} (v_{x,y} - c_1), \dots, \sum_{NN(v_{x,y})=c_k} (v_{x,y} - c_k)] \in \mathbb{R}^{L \times k}$ .

For both the query and reference images, before aggregating their conv. activations into global descriptors, we preprocess the feature maps with  $l_2$ -normalization. Since the dimensionality of the pooling and encoding features are quite different, we compress aggregated holistic features to unified dimensions with PCA dimensionality reduction for fair comparison and calculation efficiency. The final image representations are  $l_2$ -normalized again in the end with the purpose of stronger robustness against noise.

Table 1: Comparison of different aggregation methods for the last conv. layers of different CNNs. Note that the lower is the value of ANMRR the better is the accuracy and that for MAP is opposite.

(a) RS19

	Aggregation Method	CaffeNet		VGG-M		VGG-VD16		VGG-VD19		GoogLeNet	
		ANMRR	MAP(%)	ANMRR	MAP(%)	ANMRR	MAP(%)	ANMRR	MAP(%)	ANMRR	MAP(%)
Pooling	<i>Max Pooling</i>	0.353	56.90	0.316	61.49	0.286	64.38	0.288	64.29	0.274	65.51
	<i>Mean Pooling</i>	0.389	53.03	0.386	53.43	0.280	65.57	0.293	63.83	0.250	68.42
	<i>Hybrid Pooling</i>	0.350	57.31	0.316	61.59	0.284	64.65	0.286	64.57	0.269	66.05
	<i>SPoC</i>	0.411	50.53	0.412	50.21	0.294	64.17	0.312	61.84	0.263	67.18
	<i>CroW</i>	0.346	57.87	0.334	59.30	0.238	70.37	0.246	69.39	0.246	69.05
Encoding	<i>BoW</i>	0.319	61.22	0.298	63.52	0.209	73.85	0.210	73.73	<b>0.168</b>	<b>78.49</b>
	<i>IFK</i>	<b>0.244</b>	<b>69.64</b>	<b>0.233</b>	<b>71.52</b>	<b>0.190</b>	<b>76.51</b>	<b>0.188</b>	<b>76.59</b>	0.174	77.93
	<i>VLAD</i>	0.270	66.35	0.260	68.02	0.232	71.59	0.232	71.45	0.277	64.84

(b) RSSCN7

	Aggregation Method	CaffeNet		VGG-M		VGG-VD16		VGG-VD19		GoogLeNet	
		ANMRR	MAP(%)	ANMRR	MAP(%)	ANMRR	MAP(%)	ANMRR	MAP(%)	ANMRR	MAP(%)
Pooling	<i>Max Pooling</i>	0.422	46.27	0.396	49.41	0.408	47.51	0.403	47.94	0.388	49.94
	<i>Mean Pooling</i>	0.388	50.10	0.377	51.03	0.394	49.22	0.382	50.44	0.367	52.42
	<i>Hybrid Pooling</i>	0.420	46.56	0.396	49.44	0.407	47.61	0.402	48.05	0.386	50.17
	<i>SPoC</i>	0.387	49.94	0.382	50.17	0.392	48.82	0.383	49.71	0.392	49.30
	<i>CroW</i>	0.379	51.14	0.398	49.02	0.380	50.67	0.371	51.66	0.370	52.12
Encoding	<i>BoW</i>	0.378	51.54	0.375	51.87	0.368	52.29	0.360	53.22	0.354	53.86
	<i>IFK</i>	<b>0.345</b>	<b>55.51</b>	<b>0.338</b>	<b>55.79</b>	<b>0.352</b>	<b>54.01</b>	<b>0.336</b>	<b>55.61</b>	<b>0.346</b>	<b>54.97</b>
	<i>VLAD</i>	0.381	51.53	0.395	49.90	0.379	51.09	0.376	51.52	0.423	45.97

(c) UCM

	Aggregation Method	CaffeNet		VGG-M		VGG-VD16		VGG-VD19		GoogLeNet	
		ANMRR	MAP(%)	ANMRR	MAP(%)	ANMRR	MAP(%)	ANMRR	MAP(%)	ANMRR	MAP(%)
Pooling	<i>Max Pooling</i>	0.469	44.92	0.444	47.60	0.385	53.71	0.390	53.19	0.387	53.13
	<i>Mean Pooling</i>	0.535	38.75	0.495	42.22	0.413	50.81	0.416	50.22	0.381	53.94
	<i>Hybrid Pooling</i>	0.468	45.05	0.443	47.67	0.384	53.83	0.389	53.29	0.384	53.49
	<i>SPoC</i>	0.532	38.61	0.477	43.39	0.384	53.25	0.385	52.79	<b>0.339</b>	<b>58.50</b>
	<i>CroW</i>	0.493	42.85	0.473	44.63	0.376	54.94	0.379	54.36	0.349	57.26
Encoding	<i>BoW</i>	0.485	43.52	0.450	46.71	0.372	55.34	0.371	55.19	0.349	57.44
	<i>IFK</i>	<b>0.422</b>	<b>50.27</b>	<b>0.417</b>	<b>50.40</b>	<b>0.343</b>	<b>58.30</b>	<b>0.351</b>	<b>57.58</b>	0.367	55.03
	<i>VLAD</i>	0.484	43.49	0.471	44.41	0.425	49.35	0.414	50.39	0.498	39.85

### 3.1.3 Multi-scale Concatenation

Since the fusion of multi-scale information enhances the discrimination of image descriptors, we also utilize conv. features derived from images of diverse scales for there is no limit to the image size with conv. layers.

We begin with resizing the query image as well as database images to a sequence of different scales and then separately pass every scale through retrained CNN model to obtain deep features from the modified conv. layer. For any image, we receive several sets of feature maps with different sizes, and each set of feature maps are encoded into a single feature vector via aggregation method. Finally, we simply concatenate the feature vectors extracted from various scales of the same original image into an informative feature vector. These assorted features are of multiplied dimension due to vector concatenation, thus they are compressed to a unified low dimension using PCA before applied to image retrieval.

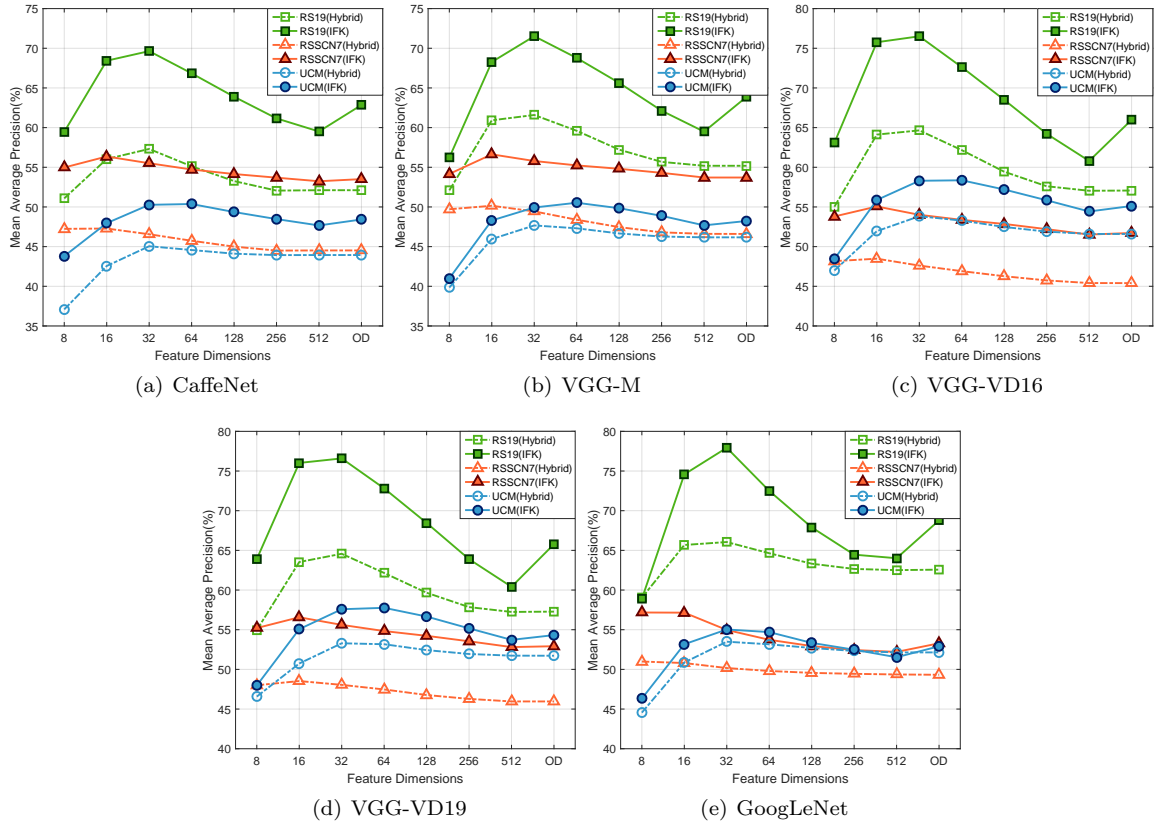


Figure 8: Performance of varying feature dimensions for both hybrid pooling and IFK on all datasets for each CNN.

## 3.2 Scheme (II): Employing FC Features

The activations derived from deep FC layers convey category-level features that can be interpreted as global representations for the input image.

When the last FC layer, namely the softmax layer, is removed, the rest portion of a CNN can be regarded as a generalized feature extractor. In contrast with conv. layers, which are able to extract features from an image of any size and aspect ratio, FC layers can only process images with a fixed size, e.g.,  $227 \times 227$  pixels or  $224 \times 224$  pixels, which is same as the size of training images. For a resized or cropped input image

$I$ , FC layers have capability of straightforwardly generating discriminating descriptors  $\mathbf{f}$  (shown in Fig. 3) that originally are in the form of single vectors of a settled dimension, which merely depends on the inherent structure of CNN model, e.g., 4096-dimension or 1024-dimension.

As with conv. layer, we carry out experiments on the first two FC layers of all CNN models adopted in our work for the sake of layer comparison. Although FC features can be directly used for similarity calculation, in order to achieve higher effectiveness, we preprocess FC activations with  $l_2$ -normalization, PCA reduction and another  $l_2$ -normalization procedure prior to implementing image retrieval.

### 3.2.1 Multi-patch Pooling

We enforce multi-patch pooling method on fine-tuned CNN model to enrich image representations with multi-position information.

We crop patches with the required size of examined CNN model at the center and four corners of an input image. Then we gather the horizontal, the vertical, coupled with the horizontal-vertical reflections of these five patches, thereby, total 20 sub-patches are generated from each image. We pass those sub-patches one by one through the first fine-tuned FC layer to extract multi-patch feature vectors, which have alike form of feature maps but have no similar spatial distribution relationship. As with conv. layers, we aggregate such 20 feature vectors into a holistic image feature using pooling method, but note that SPoC and CroW (see Sec. 3.1.1) can't be adopted because they both are spatial weighting based. Likewise, features constituted with multi-patches are PCA reduced at end.

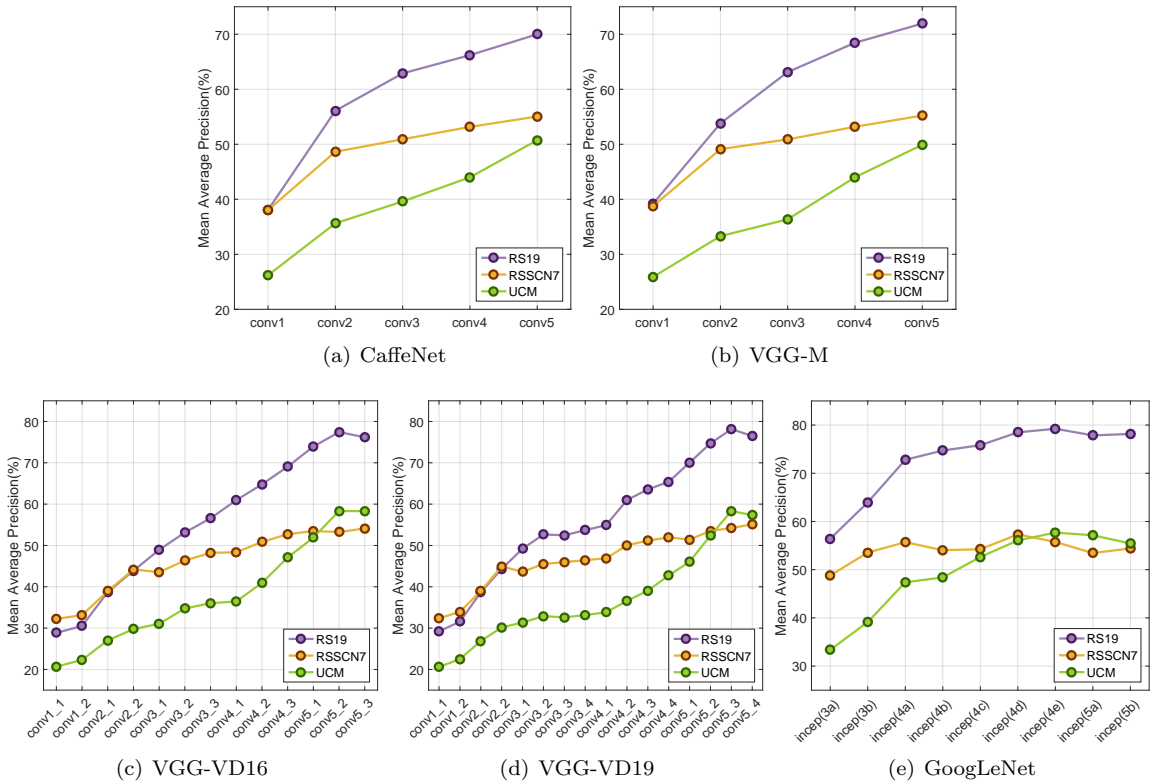


Figure 9: Performance of different conv. layers on all datasets for each CNN model. Feature maps are aggregated with IFK and final representation vectors are reduced to 32-dimension.

### 3.3 Scheme (III): Fine-tuning Off-the-shelf CNN Models

Fine-tuning is a supervised retraining process that improves the performance of CNNs for domain specific visual applications. The necessary material for fine-tuning is an annotated dataset of images relevant to the target task, and the size of this image dataset needs not to be large. The pipeline of fine-tuning is firstly initializing the CNN model other than the softmax layer with parameters optimized on a large-scale training set, next updating the parameters in part of the deeper layers or the full CNN architecture via stochastic gradient descent (SGD) using the retraining set. The dimension of the softmax layer of fine-tuned CNNs is same as the number of retraining dataset’s categories, and the remaining architecture is identical with that of the original CNNs.

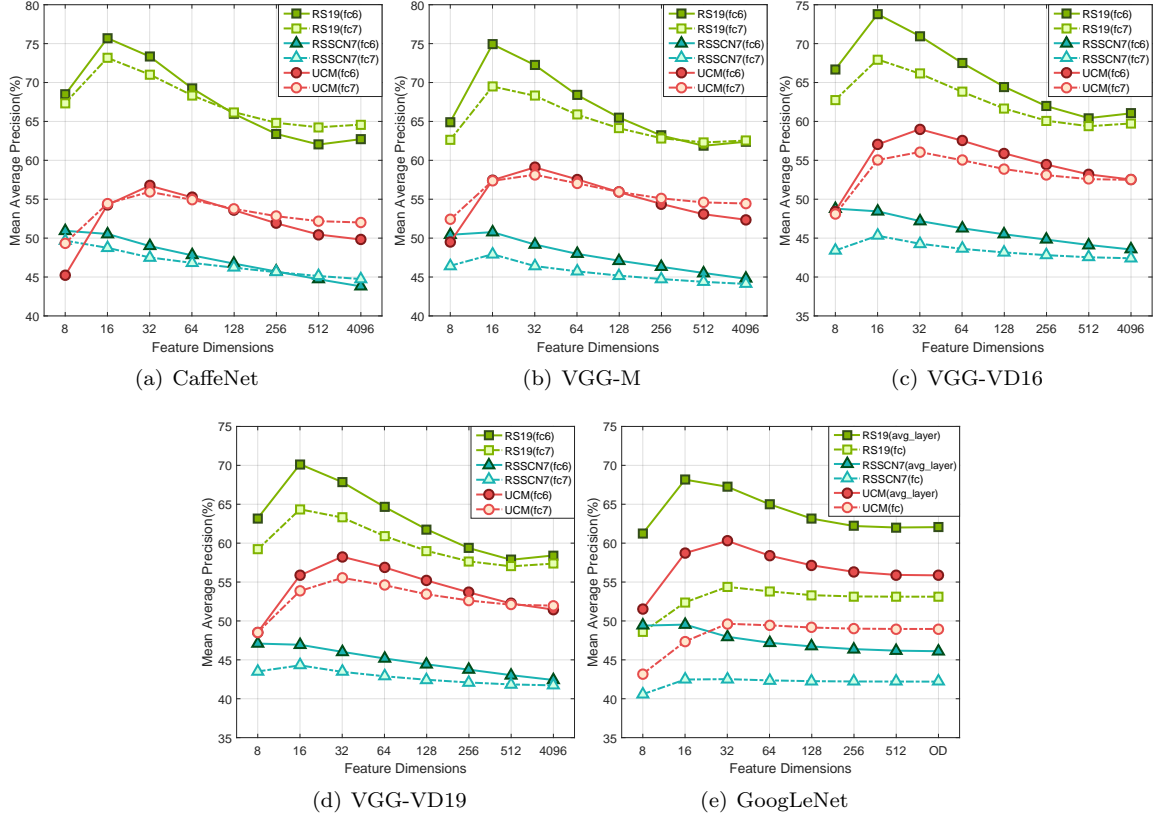


Figure 10: Performance of features from different FC layers with different dimensions on all datasets for each CNN model. “OD” means original dimensions, which are 1024 and 1000 for *avg\_layer* and *fc* in GoogLeNet respectively.

In view of the relatively large data amount and the sound data distribution of RSSCN7 [162], which is introduced in Sec. 4.1, we choose it as retraining dataset. Note that fine-tuned CNN features will be correlated with the class information of RSSCN7 by supervised learning. If such features are adopted for index, the retrieval system would incline to return images with the same class label as that of query image. However, in unsupervised retrieval issue, category labels are with no practical meaning and only used for accuracy assessment. So to avoid evaluation bias, we don’t conduct retrieval experiment with RSSCN7 fine-tuned CNNs on RSSCN7.

We intend to compare the effectiveness of conv. and FC layers in retrained CNNs, but there is no need to retrain whole CNN models on account that lower conv. layers normally perform indifferently. For

saving computing resources, we only fine-tune the last conv. layer of each CNN model except for FC layers. Specifically, for GoogLeNet, we fine-tune all 6 conv. layers between the penultimate Inception and the last Inception, as well as the last FC layer.

In actual operation, firstly we change the original 1000-dimensional softmax layer into a Gaussian distributively initialized softmax layer that contains 7 nodes, where 7 is the number of retraining dataset’s classes. Note that the CNN architecture and weights remains unchanged apart from the last output layer. Then, as with the pre-training process, we perform SGD to update the weights in layers needed to be retrained using RSSCN7. We set hyper-parameters in fine-tuning as follows: epoch number 20; mini-batch size 50; momentum 0.9; initial learning rate 0.1, which is decreased to 0.05, 0.005 and 0.001 when every 5 epochs are iterated. The variation of learning rate mitigates the validation error when it tends to convergence. Moreover, in retrained FC layers, where dropout is applied, the activations are randomly set to zero with probability 0.5 to address the problem of overfitting.

## 4 Experimental Setup

In order to explore the influence of HRRS data under the same conditions of image retrieval, we perform experiments on three publicly available HRRS image datasets: RS19 [93], RSSCN7 [162] and UCM [163]. In addition, for more comprehensive analyses, we evaluate retrieval results with several standard retrieval measures: ANMRR [164] and MAP [165]. In this section, the examined datasets, the retrieval measures, and our experimental settings are detailedly described.

### 4.1 HRRS Image Datasets

- **RS19**: The High-resolution Satellite Scene dataset is constituted by 19 categories of satellite scene images with a size of  $600 \times 600$  pixels collected on diverse orientations and scales from Google Earth. Each category contains slightly different numbers of images for a total of 1005. Example images of each class are demonstrated in Fig. 5.
- **RSSCN7**: The Remote Sensing Scene Classification dataset is composed of 7 categories of typical scene images with a size of  $400 \times 400$  pixels gathered from Google Earth. Each category contains 400 images, which are sampled on 4 different scales with 100 images per scale. Scene images in RSSCN7 are captured under changing seasons and varying weathers, combined with the mentioned mutative scales, leading to the wide variation of scenes and the challenge in image recognition. Examples from each category are displayed in Fig. 6.
- **UCM**: The UC Merced Land Use/Land Cover dataset comprises 21 categories of land-use aerial images with a size of  $256 \times 256$  pixels selected from aerial orthoimagery. Each category includes 100 images, each of which has a pixel resolution of 30cm. For certain categories, both the inter-class and inner-class diversities are relatively small, conduced to quite complexity in UCM. Samples of all categories are illustrated in Fig. 7.

### 4.2 Standard Retrieval Measures

#### 4.2.1 ANMRR

The average normalized modified retrieval rank (ANMRR) takes into account the number of ground truth items and the ranks obtained from the retrieval. Given a query image  $\mathbf{I}^q$  with a ground truth set of size  $N_g(q)$ , suppose the  $k$ -th relevant image in retrieval is found at a position  $Rank(k)$ . A penalty  $P(k)$  is assigned to items with higher rank:

$$P(k) = \begin{cases} Rank(k) & Rank(k) \leq 2N_g(q) \\ 2.5N_g(q) & Rank(k) > 2N_g(q). \end{cases} \quad (8)$$

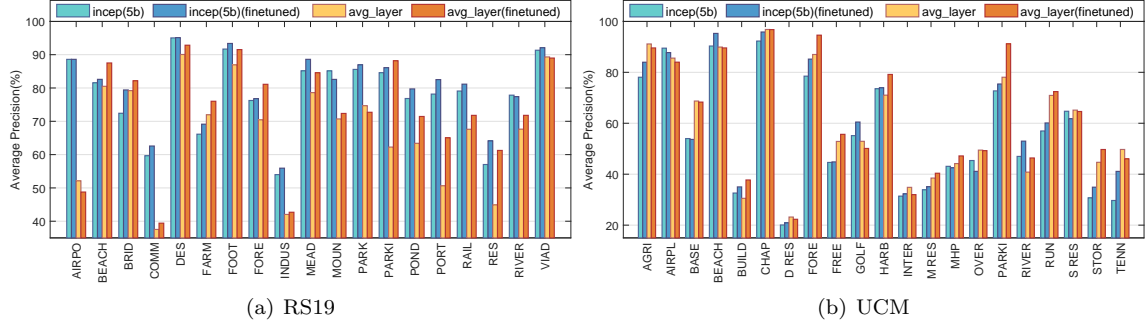


Figure 11: Per class average precision of *inception (5b)* and *avg\_layer* in pre-trained and fine-tuned GoogLeNet for both the RS19 and UCM datasets. Encoding method for conv. layer is IFK and the dimension of final feature vectors is 32.

Then the average rank (AVR) for query image  $I^q$  is calculated as:

$$AVR(q) = \frac{1}{NG(q)} \sum_{k=1}^{N_g(q)} P(k). \quad (9)$$

For minimizing the influence of variations in  $N_g(q)$ , the normalized modified retrieval rank (NMRR) is defined as:

$$NMRR(q) = \frac{AVR(q) - 0.5[1 + N_g(q)]}{2.5N_g(q) - 0.5[1 + N_g(q)]}. \quad (10)$$

The average normalized modified retrieval rank (ANMRR) can be straightforwardly acquired from NMRR for the whole set of  $N_q$  query images:

$$ANMRR = \frac{1}{N_q} \sum_{q=1}^{N_q} NMRR(q), \quad (11)$$

where  $q$  denotes the  $q$ -th query image. Note that ANMRR takes values between 0 and 1, and lower value of ANMRR indicates better retrieval performance.

#### 4.2.2 *mAP*

The mean average precision (*mAP*) is the most common way to assemble P-R curve into one value that evaluates the rank positions of all ground truth. The average precision (AvePr) for a single query image  $I^q$  is the mean over the precision scores of each relevant item:

$$AvePr(q) = \frac{1}{NG(q)} \sum_{k=1}^{NG(q)} Pr(Rank(k)). \quad (12)$$

AvePr scores of all query images finally lead to the *mAP*:

$$mAP = \frac{1}{N_q} \sum_{q=1}^{N_q} AvePr(q), \quad (13)$$

where  $N_g(q)$ ,  $Rank(k)$ ,  $NG$ ,  $k$  and  $q$  contain the same meaning as those defined in Sec. 4.2.1. Different from ANMRR, the value of MAP and the performance of retrieval system are positive correlated.

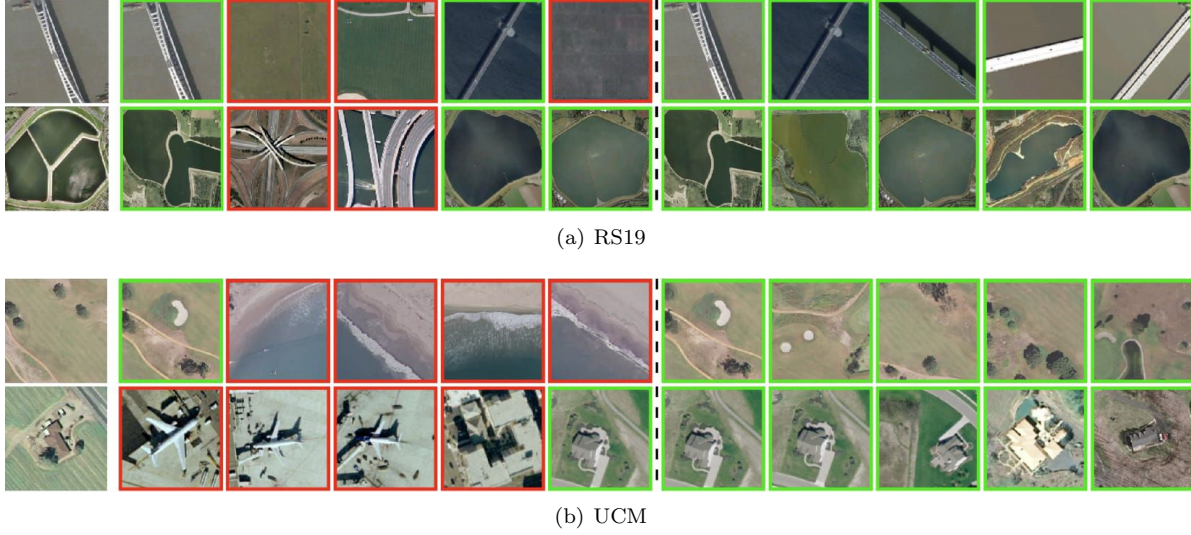


Figure 12: Retrieval results produced by original and fine-tuned GoogLeNet for the RS19 and UCM dataset. RS19 uses *inception (5b)* and UCM uses *avg\_layer*.

### 4.3 Preprocessing and Parameter Settings

In our experiments, when extracting conv. features from single scale images, we keep their original size unchanged, namely  $600 \times 600$  pixels for RS19,  $400 \times 400$  pixels for RSSCN7, and  $256 \times 256$  pixels for UCM. While FC layers can only take in images of a fixed size, hence for single FC feature extraction, we warp all images in the three datasets into  $227 \times 227$  pixels for CaffeNet, and into  $224 \times 224$  pixels for VGG-M, VGG-VD16, VGG-VD19 as well as GoogLeNet.

Particularly, in multi-scale concatenation scheme, we define each dataset to three scales as follows: for RS19, scale1, scale2 and scale3 implies for  $300 \times 300$  pixels,  $600 \times 600$  pixels and  $1200 \times 1200$  pixels respectively, here scale2 denotes the original image size; for UCM, scale1, scale2 and scale3 indicate  $256 \times 256$  pixels,  $512 \times 512$  pixels and  $1024 \times 1024$  pixels separately, yet the original size is scale1. And in multi-patch pooling scheme, since we use fine-tuned GoogLeNet, we uniformly sample sub-patches of  $224 \times 224$  pixels from both RS19 and UCM images.

We preprocess input images by subtracting the per-pixel mean value (with RGB channels) acquired from the training data for feature scaling. Whether employing conv. layers or FC layers, it is noteworthy that CNN responses are extracted after applying ReLU activation function, so that all elements are non-negative.

In the stage of conv. feature aggregation, for encoding methods, the number of K-means clustering centroids is empirically set to be 1000 and 100 respectively referring to BoW and VLAD, and the number of Gaussian components in the GMM for IFK is empirically set to be 100.

Because there is no particular query image in our experimental database, for each HRRS image dataset, we treat every image as a query and the rests from the same category as ground truth, meaning that if a retrieved image has identical class label with the query image, it will be judged as a relevant result. The final accuracies are counted after traversing a whole dataset. Apart from Sec. 5.4.1, the similarity measure we use in experiments is Euclidean distance.

## 5 Results and Analyses

In this section, we display the results of HRRS image retrieval experiments and analyze the effects of overall variables on retrieval performance. These variables cover aspects as follows: architecture of pre-trained CNN, depth of CNN layer, aggregation method for convolutional layers, dimension of feature vector and fine-tuning. We perform comprehensive experiments based on deep CNN models.

In all of the following experiments, CNN layers are denoted using their numerical orders, such as “*conv5*”, “*conv5\_3*” referring to conv. layers and “*fc6*”, “*fc7*” referring to FC layers, which are illustrated in Fig. 2 at length.

### 5.1 Convolutional Layers

#### 5.1.1 Aggregation Method

We first examine the performance of various aggregation methods used for conv. layers. For both the query image and dataset images, we keep their size unchanged to compute the forward propagation activations and extract feature maps from the last conv. layer of each examined pre-trained CNN model. We apply both encoding (i.e., BoW, IFK and VLAD) and pooling (i.e., Max, Mean, Hybrid, SPoC and CroW) methods to transform feature maps into global feature vectors, all of which are finally compressed to 32-dimensional vectors using PCA before similarity calculation.

The performance comparisons of different aggregation methods as well as different CNN models are shown in Table 1, which demonstrates that the best results for the RS19, RSSCN7, and UCM datasets are severally obtained by adopting GoogLeNet with BoW, achieving MAP of 78.49%; VGG-M with IFK, achieving MAP of 55.79%; and GoogLeNet with SPoC, achieving MAP of 58.50%. Whereas it can be clearly observed that informative IFK generally outstands among all aggregation methods, and GoogLeNet normally outperforms other CNNs based on its deep architecture. This shows that in most cases, sophisticated encoding method is capable of generating discriminating image features.

#### 5.1.2 Dimensionality Reduction

Here we explore the impact of image feature dimensions on retrieval performance, while comparing different variation tendencies of MAP when applying encoding and pooling methods. We use hybrid pooling and IFK on feature maps yielded by the last conv. layers of different CNNs, and then reduce each feature vector with PCA to some continuously changed dimensions:  $\{8, 16, 32, 64, 128, 256, 512, \dots\}$ . The dimension of hybrid pooling features is the maximum among all pooling features (it is the concatenation of max pooling and mean pooling) so that hybrid pooling enables us to test on a wider range of varying dimensions.

We plot the change curves of MAP for different PCA compression rates in Fig. 8, where “OD” denotes original dimensions, namely we do not perform PCA on such feature vectors. In practical terms, for CaffeNet, the original dimensions of Hybrid and IFK features are 512 and 51200 severally; for VGG-M and VGG-VD, the original dimensions of Hybrid and IFK features are 1024 and 102400; and for GoogLeNet, the original dimensions of Hybrid and IFK features are 2048 and 204800 respectively.

Apparently, the best accuracies for all datasets and methods are consistently achieved when feature dimensions are in the range of 16-64, illustrating that although reduced image representations retain less information, they can even do better than uncompressed vectors in retrieval task. Perhaps because the discarded secondary components carry redundant information and are useless for image retrieval. In contrast to hybrid pooling, MAP of IFK is distinctly higher and changes more violently when feature dimension is increasing. These observations indicate that PCA compression not only saves computational resources in a smaller memory footprint but also can make progress for retrieval effectiveness.

Table 2: Performance of multi-scale concatenation method applied on retrained GoogLeNet. Feature maps are encoded via BoW.

Dataset	Single Scale			Multiple Scales			
	Scale1	Scale2	Scale3	Scale(1,2)	Scale(1,3)	Scale(2,3)	Scale(1,2,3)
RS19	78.95	81.08	68.47	<b>82.53</b>	69.67	72.84	73.70
UCM	<b>58.69</b>	50.04	35.30	52.97	36.14	37.83	38.49

Table 3: Performance of multi-patch pooling method applied on retrained GoogLeNet. Accuracy is measured on MAP.

Dataset	Full-size Image	Multiple Patches		
	Single feature	Max pooling	Mean pooling	Hybrid pooling
RS19	72.96	75.62	<b>76.80</b>	76.01
UCM	62.23	63.57	<b>64.56</b>	63.93

### 5.1.3 Depth of CNN Layer

We wish to confirm which conv. layer suits best for retrieval task. Therefore, we make use of IFK to encode feature maps extracted by all conv. layers of each CNN model and compress the consequent feature vectors to 32-dimension uniformly. Fig. 9 shows MAP evaluated from the corresponding conv. layers.

For CaffeNet and VGG-M, architectures of which are relatively shallow, MAP keeps rising along with the depth of layers on all three datasets, and achieves the highest value at *conv5*. For very deep nets, i.e. VGG-VD16 and VGG-VD19, MAP of the RS19 and UCM datasets increases until reaching a peak at the penultimate layer, *conv5\_2* and *conv5\_3* respectively, then drops slightly as layers go deeper. However, different from the other two datasets, the best results of RSSCN7 are obtained at the last conv. layer *conv5\_3* and *conv5\_4* separately for VGG-VD16 and VGG-VD19 rather than intermediate layers. As to GoogLeNet, it is apparent that MAP trends much more smoothly as the change of layer depth, and the best performing layers on every dataset are all intermediate layers: *inception(4e)* behaves best for RS19 and UCM, and *inception(4d)* outperforms for RSSCN7. In contrast to other very deep nets, the most suitable layer for RSSCN7 is shallower than those of others in GoogLeNet.

Our experiments demonstrate that, deeper layers usually perform better for retrieval task, since every activation on feature maps obtained from deeper layers corresponds to bigger receptive field, which lead to more information of original image. But different from classification task, performance of retrieval is not always optimized by deeper layers of CNNs, especially for which are very deep in structure. Because for the deepest conv. layer in very deep nets, the receptive field represented by single response element is of a considerable large scale and unable to grasp the details. Although image representations captured by deeper layers are more abstract and global, they are likely to lose information of fine-grained local textures and objects, as well as become less discriminative for retrieval.

## 5.2 Full-connected Layers

### 5.2.1 Dimensionality Reduction

We also conduct retrieval experiments for FC layers. We resize both the query image and database images to required resolution of CNNs before extracting deep features. Outputs of FC layers are single vectors, length of which is 4096 except for that of GoogLeNet. Especially for GoogLeNet, dimensions of *avg.layer* and *fc* are 1024 and 1000 respectively.

We as well compress feature vectors from FC layers to diverse dimensions by PCA to investigate the effect of dimensionality reduction. It can be seen in Fig. 10 that PCA compression similarly improves the

Table 4: Comparisons between conv. and FC layers of all CNNs for all dataset. Feature maps from conv. layers are aggregated by IFK. Note that the lower is the value of ANMRR the better is the accuracy, that for MAP is opposite.

CNN Model	RS19				RSSCN7				UCM			
	Layer	Dim	ANMRR	MAP(%)	Layer	Dim	ANMRR	MAP(%)	Layer	Dim	ANMRR	MAP(%)
CaffeNet	conv5	32	0.241	69.90	conv5	16	0.341	55.78	conv5	32	0.416	50.73
	fc6	16	0.190	75.70	fc6	8	0.376	50.94	fc6	32	0.364	56.74
VGG-M	conv5	32	0.230	71.94	conv5	16	0.337	55.99	conv5	64	0.419	50.51
	fc6	16	0.197	74.91	fc6	16	0.383	50.77	fc6	32	0.340	59.09
VGG-VD16	conv5_2	16	0.174	78.52	conv5_3	16	0.340	55.30	conv5_2	32	0.350	58.34
	fc6	16	0.203	73.79	fc6	8	0.393	48.79	fc6	32	0.339	59.00
VGG-VD19 <small>table:II</small>	conv5_3	16	<b>0.163</b>	<b>79.48</b>	conv5_4	16	0.331	56.12	conv5_3	64	0.349	58.44
	fc6	16	0.232	70.14	fc6	8	0.409	47.09	fc6	32	0.345	58.25
GoogLeNet	inception(4e)	32	0.165	79.24	inception(4d)	16	<b>0.314</b>	<b>59.04</b>	inception(4e)	64	0.349	57.97
	avg_layer	16	0.243	68.16	avg_layer	16	0.387	49.53	avg_layer	32	<b>0.320</b>	<b>60.29</b>

Table 5: Comparisons between original and retrained CNNs on RS19 and UCM with MAP.

Dataset	Layer Type	CaffeNet		VGG-M		VGG-VD16		GoogLeNet	
		Original	Finetuned	Original	Finetuned	Original	Finetuned	Original	Finetuned
RS19	Conv.	69.90	70.13	71.94	72.51	76.18	77.20	78.16	<b>80.21</b>
	FC	73.35	75.47	72.25	75.55	70.97	75.79	67.25	72.96
UCM	Conv.	50.73	51.71	49.91	52.06	58.30	59.96	55.44	57.82
	FC	56.74	58.93	59.09	61.99	59.00	61.97	60.29	<b>62.23</b>

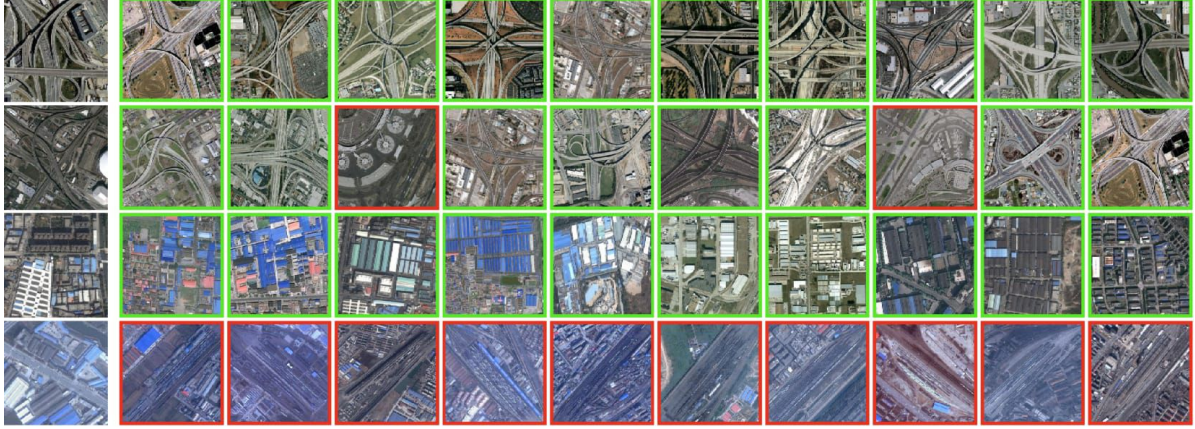
retrieval performance for FC layers of all CNNs. The optimized dimensions for the RS19 and UCM datasets are with respect to 16 and 32 for all CNN models. While for RSSCN7, MAP becomes highest when image representations are with dimensions of 8 for CaffeNet, VGG-VD16, VGG-VD19, and of 16 for VGG-M, GoogLeNet. These experimental phenomena demonstrated that PCA compression is also effective for FC features in performance improvement.

### 5.2.2 Depth of CNN Layer

As with conv. layers, we perform retrieval test on every FC layer of each CNN model. Fig. 10 clearly illustrated that the peak of MAP of every dataset is achieved by the lower layer whatever the CNN model is, where “OD” still means original dimensions: 1024 and 1000 for feature vectors drawn from *avg\_layer* and *fc* of GoogLeNet respectively. It is verified again that the deeper layers are not always the better since representations from deeper layers may be too semantically specific to pre-training natural dataset. Whereas for CaffeNet and VGG-M, *fc7* sometimes wins out when feature dimensions are relatively high. For VGG-VD16 and VGG-VD19, MAP of *fc7* grows closer to that of *fc6* as dimension increases. And for GoogLeNet, *avg\_layer* constantly surpass *fc* by a large gap no matter how the dimension of image features changes.

### 5.2.3 Convolutional vs Full-connected

We intend to carry out an overall comparison between conv. layers and FC layers. We firstly pick out layers offering the highest MAP from both conv. and FC layers for each CNN and each dataset, as well as the dimension which wins out for each selected layer, and then exhibit a comprehensive assessment in Table 4. The aggregation method here to encode conv. features is also IFK. In this table, except for accuracy evaluation, the best layers and the best dimensions are also displayed, where “Dim” is the abbreviation of dimension. The greatest accuracies of the RS19, RSSCN7 and UCM datasets are respectively obtained by *conv5\_3* in VGG-VD19 with MAP value of 79.48%, *inception (4d)* in GoogLeNet with MAP value of 59.04%,



(a) RS19



(b) UCM

Figure 13: Qualitative retrieval results of both RS19 and UCM. We select the best method for RS19 and UCM, and pick out the images with the highest and lowest precision in the class with the highest and lowest average precision, which means 4 query images for each dataset.

and *avg\_layer* in GoogLeNet with MAP value of 60.29%. More generally, in most cases, features from conv. layers are more outstanding for the RS19 and RSSCN7 datasets though features from FC layers works better for UCM.

### 5.3 Fine-tuning CNN Model

For the purpose of comparing pre-trained and fine-tuned CNN models, we partially retrain the last conv. layer and all FC layers of experimental CNNs using RSSCN7 and then experiment modified CNN models on RS19 and UCM.

The quantitative evaluation with MAP is shown in Table 5, we use the last conv. layer and the first FC layer of each CNN for feature extraction and apply PCA to reduce all image representations to 32-dimension. IFK is the unified aggregation method for conv. feature maps on account of its prominent performance testified in Table 1. It can be observed that all fine-tuned models consistently produce better MAP on both test datasets whether conv. layers or FC layers are used. The biggest advancements are severally obtained

by *fc* in GoogLeNet for RS19 with an increase of 5.71% on MAP, and by *fc6* in VGG-VD16 for UCM with an increase of 2.97% on MAP. And the overall best accuracies of the RS19 and UCM datasets are respectively generated by *inception (5b)* in fine-tuned GoogLeNet with MAP value of 80.21%, and *avg\_layer* in fine-tuned GoogLeNet with MAP value of 62.23%, as observed in the previous experiments, GoogLeNet still behaves best even though being fine-tuned.

For further analysis on the influence of fine-tuning, we make use of per-class bar graph to estimate retrieval accuracy. In this section, we conduct evaluation particularly on pre-trained and retrained GoogLeNet for its remarkable performance. Fig. 11 illustrates average precision of each class resulting from RS19 and UCM.

Fig. 11 demonstrates that, for RS19, accuracies of most categories are improved after fine-tuning, except for the classes of *airport*, *park* and *river*. The number of classes in UCM that perform worse or unchangeably is more than that of RS19 because of categorical attributes of the retraining data RSSCN7. The RSSCN7 dataset only contains 7 classes, which can not cover the 19 classes of RS19 or 21 classes of UCM. In addition, image properties in same categories of the three datasets are distinctly different. In this sense, although fine-tuning is able to enhance the transferability of off-the-shelf CNN models and make CNNs work better for specific tasks at hand, performance of each category can't always improve on account of data discrepancy.

At last, we display two sets of qualitative retrieval results in Fig. 12, from left to right displayed the top 5 images retrieved with original and fine-tuned GoogLeNet. Since the best performance on RS19 and UCM is derived by different layers in Table 5, here we specially show the results of *inception (5b)* for RS19 and the results of *avg\_layer* for UCM. There is no doubt that the retrained CNN model performs better. Pay attention to query pond image in Fig. 12(a), pre-trained GoogLeNet notices its cross structure over the water so returns a few viaduct images, which include cross structure but are erroneous results. However, when pre-train GoogLeNet with HRRS images, modified convolution filters are capable of capturing more specific semantic information of HRRS images, therefore fine-tuned CNN can retrieve correct images even when the significant structures of query and relevant images are different.

In Fig. 12(b) retrieved beach images have similar curve texture with the query meadow image hence they are searched from dataset as wrong results. Although structure and texture can always determine integrity attribute of natural images, HRRS images formed by analogical structure and texture are likely to contain completely different semantic properties so that fine-tuning can make CNNs more suitable for HRRS image retrieval.

The above experiments suggest that fine-tuning operation is able to reinforce the transferability of CNNs. Despite an off-the-shelf CNN model already has strong capability of generalization, the particular property of training data still somewhat limits CNN's competence. Retraining CNNs using dataset that is relevant to the interest task will further professionalize them to address domain specific applications.

## 5.4 Multi-scale Concatenation and Multi-patch Pooling

### 5.4.1 Multi-scale Concatenation

On the basis of the above experiments, we further explore how multiple scales of input images impact on retrieval results. We resize both query image and reference images into continuously varying scales: *scale1*, *scale2*, and *scale3*, which are defined respectively for RS19 and UCM in Sec. 4.3, and then pass them through fine-tuned GoogLeNet to obtain multi-scale feature maps from *inception(5b)*. Apart from single scale, we simply concatenate global features of different scales for more informative image representations, signified as *scale(1,2)*, *scale(1,3)*, *scale(2,3)* and *scale(1,2,3)*. Take note that the encoding method we apply here is BoW instead of IFK, partly because BoW has shown great performance that is not lost to IFK on GoogLeNet in Table 1. On the other hand, *inception(5b)* contain 1024 feature maps, leading to single-scale IFK features with a dimension of 204800, whereas BoW features are merely 1000-dimensional, so in view of memory efficiency, BoW is more suitable in the context of feature vector concatenation. At last, different dimensional single and multiple scale feature vectors are uniformly compressed to be 32-dimensional by PCA.

Table 2 presents resulting MAP on RS19 and UCM. For single scale image representations, the finest *scale1*

Table 6: Comparison with the current methods. The comparison is based on several distance measures and evaluated by ANMRR, which indicates better performance with lower value. “Dim” means the dimension of image feature vector.

Descriptors	Dim	Similarity Metrics			
		Euclidean	Cosine	Manhattan	Chi-square
CCH+RIT+FPS <sub>1</sub> +FPS <sub>2</sub> [69]	62	0.640	-	0.589	0.575
CCH+RIT (BoW) [110]	128	0.640	-	0.613	0.585
Salient SIFT (BoW) [109]	128	0.607	0.607	0.591	0.599
Dense SIFT(VLAD) [114]	25600	-	0.460	-	-
Pyramid LPS-aug [112]	-	0.472	-	-	-
Manual RF VGG-M [75]	4096	0.316	0.316	0.333	0.315
Fine-tuned VGG-M [74]	4096	0.299	-	-	-
GoogLeNet(finnetuned)+BoW	1000	0.423	0.423	0.685	0.639
GoogLeNet(finnetuned)+MultiPatch	1024	0.314	0.314	0.323	<b>0.309</b>
GoogLeNet(finnetuned)+BoW+PCA	32	0.335	0.335	0.337	-
GoogLeNet(finnetuned)+MultiPatch+PCA	32	<b>0.285</b>	<b>0.285</b>	<b>0.303</b>	-

achieves the best accuracy of 58.69% on UCM and the relatively larger scale2 performs better on RS19, while the largest scale3 behaves worst for both two datasets. The property of single scale features evidently affects the discrimination of multi-scale representations, all of combinations with scale3 produce very poor MAP on both datasets, and multi-scale concatenation doesn’t even do UCM any favors. Nevertheless, on RS19, scale(1,2) acquires the overall highest MAP of 82.53%, which is ahead of the best single scale accuracy of 81.08%.

An intuitive explanation for such experimental phenomena is that the scale of receptive field corresponding to each activation over feature maps varies with the scale of input image, since the size of the convolutional filters in CNNs remain unchanged. CNN activations focus more on global semantic information for images of finer scale, yet capturing local details from large scale input images. It again makes sense that RS19 and UCM are quite different in nature, RS19 is sensitive to low level visual features, such as edges, texture and graph structure, while UCM tends to be object-oriented. Hence the combinations of enlarged scales even detract the discriminating ability of image representations for UCM, only to gather the appropriate features can information enrichment push forward the retrieval performance.

#### 5.4.2 Multi-patch Pooling

We validate the effect of multi-patch pooling by cropping 20 sub-patches of  $224 \times 224$  pixels from corner and center in each input image and extracting deep features from *avg\_layer* of retrained GoogLeNet. Sets of feature vectors associated to different locations are compressed into compact representations via max pooling, mean pooling and hybrid pooling, before implementing retrieval, all features are reduced into a dimension of 32 using PCA.

As displayed in Table 3, multi-patch pooling significantly boosts the performance on MAP compared to the second column, which shows retrieval accuracy of single feature vectors drawn from warped full-size images. Remark that the best results on RS19 and UCM are both acquired by mean pooling, with MAP of 76.80% and 64.56% respectively, indicating that mean pooling is the most efficient in terms of multi-patch information fusion.

According to our experimental results, the overall highest MAP for RS19 is 82.53% achieved by scale(1,2) concatenation using *inception(5b)* from fine-tuned GoogLeNet, and for UCM is 64.56% obtained by multi-patch mean pooling using *avg\_layer* from fine-tuned GoogLeNet. To give a sense of qualitative analysis on

our best performing scheme, we pick out the categories with the highest and lowest average precision from RS19 and UCM on the basis of the above two methods separately. The best and worst performing categories for RS19 are *viaduct* and *industrial* respectively, and for UCM are *chaparral* and *dense residential*. Then we seek out query images with the highest and lowest retrieval precision among those classes, and demonstrate top 10 retrieved results in Fig. 13. For each dataset, the best and worst queries in the best class lie on the first and second row, and those in the worst class lie on the third and fourth row.

The best query images from all classes present excellent qualitative results in expectation, however, the worst *industrial*, *chaparral* and *dense residential* queries search out few or no correct images. Notable observation is that the false retrieval results are similar to the queries in prominent edge and local texture, such as falsely retrieved *railway station* images with their *industrial* query, and falsely retrieved *forest* images with their *chaparral* query. This phenomenon can be attribute to the semantic gap existing between the image representations and the visual content conveyed by HRRS images.

## 5.5 Comparison with the current methods

We compare our proposed schemes with the recent HRRS image retrieval methods in Table 6. Because relative works are almost all assessed on UCM, we only compare the retrieval accuracies of one dataset. We select methods yielding the highest MAP on UCM from Table 3 and Table 2, namely using BoW to encode *inception(5b)* layer features derived from single scale1, and adopting multi-patch mean pooling on *avg\_layer* of fine-tuned GoogLeNet.

We evaluate the performance of retrieval using ANMRR on several distance metrics: Euclidean, Cosine, Manhattan and  $\chi^2$ -square, besides accuracy, we also compare the dimensions of image representations, which is closely connected to computational efficiency. On account of  $\chi^2$ -square distance’s computational condition that elements of the feature vectors must be non-negative, we omitted the ANMRR of dimensionality compressed descriptors in Table 6 since PCA reduction may make vector elements to become negative.

Comparative methods are based on hand-crafted features or basic deep features, [69] exploits the combination of several global morphological texture descriptors, [109] and [114] respectively apply BoW and VLAD encoding methods on salient and dense SIFT features to obtain global descriptors, [112] obtains global features by encoding local pattern spectra with VLAD, [75] simply utilizes deep features extracted from the first FC layer of VGG-M coupled with manual relevant feedback, and [74] extracts FC features from fine-tuned VGG-M model.

It is apparently that on any kind of distance metric, our methods always outperform all other methods. Especially, the overall best accuracy is acquired by compressed multi-patch mean pooling on Euclidean distance with ANMRR value of 0.285, which is about 1.4% lower than the recent CNN-based method [74]. Apart from the precision, the feature dimension of our method is the lowest, standing for distinctly decrease in the computation cost.

## 6 Conclusion

In this paper, we have comprehensively reviewed existing research works on content-based RS image retrieval and explored how to use CNNs to solve HRRS image retrieval issue by carrying out a sequence of systematical experiments. We take exhaustive factors that may impact the performance of image retrieval into account and experimented on three public HRRS image datasets with five representative CNN models. Factors that are relative to the discrimination of image representations include structure of CNNs, depth of CNN layers, aggregation methods, dimensionality reduction, fine-tuning operation and information enrichment.

We methodically propose four experimental schemes: aggregating feature maps drawn from conv. layers, directly utilizing feature vectors derived from FC layers, enforcing fine-tuning strategy on pre-trained CNNs, and implement multi-scale concatenation or multi-patch pooling methods. By optimizing and analyzing influence variables through such four schemes, we have achieved outstanding retrieval performance on examined

HRRS image datasets: overall MAP value of 82.53% for RS19 and 64.56% for UCM respectively (RSSCN7 is used for fine-tuning). Particularly on UCM, our retrieval method surpasses previous state-of-the-art with reducing ANMRR by about 3.1%.

## References

- [1] H. Lotz-Iwen and W. Steinborn, “The intelligent satellite-image information system isis,” in *AIP Conference Proceedings*, vol. 283, no. 1. AIP, 1993, pp. 727–734.
- [2] C. Chang, B. Moon, A. Acharya, C. Shock, A. Sussman, and J. H. Saltz, “Titan: A high-performance remote sensing database,” in *Proceedings of the Thirteenth International Conference on Data Engineering, April 7-11, 1997 Birmingham U.K.*, 1997, pp. 375–384.
- [3] C. Faloutsos, R. Barber, M. Flickner, J. Hafner, W. Niblack, D. Petkovic, and W. Equitz, “Efficient and effective querying by image content,” *J. Intell. Inf. Syst.*, vol. 3, no. 3/4, pp. 231–262, 1994.
- [4] V. N. Gudivada and V. V. Raghavan, “Content-based image retrieval systems - guest editors’ introduction,” *IEEE Computer*, vol. 28, no. 9, pp. 18–22, 1995.
- [5] K. Seidel, R. Mastropietro, and M. Datcu, “New architectures for remote sensing image archives,” in *Geoscience and Remote Sensing, 1997. IGARSS’97. Remote Sensing-A Scientific Vision for Sustainable Development., 1997 IEEE International*, vol. 1. IEEE, 1997, pp. 616–618.
- [6] K. Seidel, M. Schroder, H. Rehrauer, G. Schwarz, and M. Datcu, “Query by image content from remote sensing archives,” in *Geoscience and Remote Sensing Symposium Proceedings, 1998. IGARSS’98. 1998 IEEE International*, vol. 1. IEEE, 1998, pp. 393–396.
- [7] M. Datcu and K. Seidel, “Image information mining: exploration of image content in large archives,” in *Aerospace Conference Proceedings, 2000 IEEE*, vol. 3. IEEE, 2000, pp. 253–264.
- [8] G. B. Marchisio, W.-H. Li, M. Sannella, and J. R. Goldschneider, “Geobrowse: an integrated environment for satellite image retrieval and mining,” in *Geoscience and Remote Sensing Symposium Proceedings, 1998. IGARSS’98. 1998 IEEE International*, vol. 2. IEEE, 1998, pp. 669–673.
- [9] K. Koperski, G. Marchisio, S. Aksoy, and C. Tusk, “Visimine: Interactive mining in image databases,” in *Geoscience and Remote Sensing Symposium, 2002. IGARSS’02. 2002 IEEE International*, vol. 3. IEEE, 2002, pp. 1810–1812.
- [10] K. W. Tobin, B. L. Bhaduri, E. A. Bright, A. M. Cheriyyadat, T. P. Karnowski, P. J. Palathingal, T. E. Potok, and J. R. Price, “Large-scale geospatial indexing for image-based retrieval and analysis,” in *Advances in Visual Computing, First International Symposium, ISVC 2005, Lake Tahoe, NV, USA, December 5-7, 2005, Proceedings*, 2005, pp. 543–552.
- [11] K. W. Tobin, B. L. Bhaduri, E. A. Bright, A. Cheriyyadat, T. P. Karnowski, P. J. Palathingal, T. E. Potok, and J. R. Price, “Automated feature generation in large-scale geospatial libraries for content-based indexing,” *Photogrammetric Engineering & Remote Sensing*, vol. 72, no. 5, pp. 531–540, 2006.
- [12] M. Klaric, G. Scott, C.-R. Shyu, C. Davis, and K. Palaniappan, “A framework for geospatial satellite imagery retrieval systems,” in *Proc. Int. Geosci. and Remote Sens. Symp*, 2006, pp. 2457–2460.
- [13] C.-R. Shyu, M. Klaric, G. J. Scott, A. S. Barb, C. H. Davis, and K. Palaniappan, “Geoiris: Geospatial information retrieval and indexing systemcontent mining, semantics modeling, and complex queries,” *IEEE Transactions on geoscience and remote sensing*, vol. 45, no. 4, pp. 839–852, 2007.

- [14] M. Datcu, K. Seidel, S. D’Elia, and P. Marchetti, “Knowledge-driven information mining in remote-sensing image archives.” *E. S. A. Bulletin*, no. 110, pp. 26–33, 2002.
- [15] M. Datcu, H. Daschiel, A. Pelizzari, M. Quartulli, A. Galoppo, A. Colapicchioni, M. Pastori, K. Seidel, P. G. Marchetti, and S. d’Elia, “Information mining in remote sensing image archives: system concepts,” *IEEE Trans. Geoscience and Remote Sensing*, vol. 41, no. 12, pp. 2923–2936, 2003.
- [16] H. Daschiel and M. Datcu, “Information mining in remote sensing image archives: system evaluation,” *IEEE Trans. Geoscience and Remote Sensing*, vol. 43, no. 1, pp. 188–199, 2005.
- [17] I. M. G. Muñoz and M. Datcu, “System design considerations for image information mining in large archives,” *IEEE Geoscience and Remote Sensing Letters*, vol. 7, no. 1, pp. 13–17, 2010.
- [18] M. Molinier, J. Laaksonen, J. Ahola, and T. Häme, “Self-organizing map application for retrieval of man-made structures in remote sensing data,” in *Proc. ESA-EUSC Workshop on Image Information Mining-Theory and Application to Earth Observation, Frascati, Italy*, 2005.
- [19] T. Zhang, W. Yan, C. Su, and S. Ji, “Accurate object retrieval for high-resolution remote-sensing imagery using high-order topic consistency potentials,” *International Journal of Remote Sensing*, vol. 36, no. 16, pp. 4250–4273, 2015.
- [20] S. S. Durbha and R. L. King, “Semantics-enabled framework for knowledge discovery from earth observation data archives,” *IEEE Transactions on geoscience and remote sensing*, vol. 43, no. 11, pp. 2563–2572, 2005.
- [21] F. Dell’Acqua and P. Gamba, “Query-by-shape in meteorological image archives using the point diffusion technique,” *IEEE transactions on geoscience and remote sensing*, vol. 39, no. 9, pp. 1834–1843, 2001.
- [22] I. E. Alber, Z. Xiong, N. Yeager, M. Farber, and W. M. Pottenger, “Fast retrieval of multi-and hyperspectral images using relevance feedback,” in *Geoscience and Remote Sensing Symposium, 2001. IGARSS’01. IEEE 2001 International*, vol. 3. IEEE, 2001, pp. 1149–1151.
- [23] L. Gueguen, M. Pesaresi, and P. Soille, “An interactive image mining tool handling gigapixel images,” in *Geoscience and Remote Sensing Symposium (IGARSS), 2011 IEEE International*. IEEE, 2011, pp. 1581–1584.
- [24] A. Julea, N. Méger, P. Bolon, C. Rigotti, M.-P. Doin, C. Lasserre, E. Trouvé, and V. N. Lazarescu, “Unsupervised spatiotemporal mining of satellite image time series using grouped frequent sequential patterns,” *IEEE Transactions on Geoscience and Remote Sensing*, vol. 49, no. 4, pp. 1417–1430, 2011.
- [25] T.-B. Jiang, G.-S. Xia, Q.-K. Lu, and W.-M. Shen, “Retrieving aerial scene images with learned deep image-sketch features,” *Journal of Computer Science and Technology*, vol. 32, no. 4, pp. 726–737, 2017.
- [26] A. Vellaikal, C. J. Kuo, and S. K. Dao, “Content-based retrieval of remote-sensed images using vector quantization,” in *Visual Information Processing IV, Orlando, FL, USA, April 17, 1995*, 1995, pp. 178–189.
- [27] J. E. Barros, J. C. French, W. N. Martin, and P. M. Kelly, “System for indexing multispectral satellite images for efficient content-based retrieval,” in *IS&T/SPIE’s Symposium on Electronic Imaging: Science & Technology*. International Society for Optics and Photonics, 1995, pp. 228–237.
- [28] G. Healey and A. Jain, “Retrieving multispectral satellite images using physics-based invariant representations,” *IEEE Trans. Pattern Anal. Mach. Intell.*, vol. 18, no. 8, pp. 842–848, 1996.

- [29] K. Seidel, M. Schroder, H. Rehrauer, and M. Datcu, "Meta features for remote sensing image content indexing," in *Geoscience and Remote Sensing Symposium Proceedings, 1998. IGARSS'98. 1998 IEEE International*, vol. 2. IEEE, 1998, pp. 1022–1024.
- [30] M. Datcu, K. Seidel, and M. Walessa, "Spatial information retrieval from remote-sensing images. i. information theoretical perspective," *IEEE transactions on geoscience and remote sensing*, vol. 36, no. 5, pp. 1431–1445, 1998.
- [31] M. Schroder, H. Rehrauer, K. Seidel, and M. Datcu, "Spatial information retrieval from remote-sensing images. ii. gibbs-markov random fields," *IEEE Transactions on geoscience and remote sensing*, vol. 36, no. 5, pp. 1446–1455, 1998.
- [32] M. Schröder, M. Walessa, H. Rehrauer, K. Seidel, and M. Datcu, "Gibbs random field models: a toolbox for spatial information extraction," *Computers & Geosciences*, vol. 26, no. 4, pp. 423–432, 2000.
- [33] T. Bretschneider and O. Kao, "A retrieval system for remotely sensed imagery," in *International Conference on Imaging Science, Systems, and Technology*, vol. 2, 2002, pp. 439–445.
- [34] T. Bretschneider, R. Cavet, and O. Kao, "Retrieval of remotely sensed imagery using spectral information content," in *Geoscience and Remote Sensing Symposium, 2002. IGARSS'02. 2002 IEEE International*, vol. 4. IEEE, 2002, pp. 2253–2255.
- [35] Y. Hongyu, L. Bicheng, and C. Wen, "Remote sensing imagery retrieval based-on gabor texture feature classification," in *Signal Processing, 2004. Proceedings. ICSP'04. 2004 7th International Conference on*, vol. 1. IEEE, 2004, pp. 733–736.
- [36] S. Newsam, L. Wang, S. Bhagavathy, and B. S. Manjunath, "Using texture to analyze and manage large collections of remote sensed image and video data," *Applied optics*, vol. 43, no. 2, pp. 210–217, 2004.
- [37] A. Ma and I. K. Sethi, "Local shape association based retrieval of infrared satellite images," in *Seventh IEEE International Symposium on Multimedia (ISM 2005), 12-14 December 2005, Irvine, CA, USA, 2005*, pp. 551–557.
- [38] S. D. Newsam and Y. Yang, "Comparing global and interest point descriptors for similarity retrieval in remote sensed imagery," in *15th ACM International Symposium on Geographic Information Systems, ACM-GIS 2007, November 7-9, 2007, Seattle, Washington, USA, Proceedings, 2007*, p. 9.
- [39] P. Agouris, J. Carswell, and A. Stefanidis, "An environment for content-based image retrieval from large spatial databases," *ISPRS Journal of Photogrammetry and Remote Sensing*, vol. 54, no. 4, pp. 263–272, 1999.
- [40] V. P. Shah, N. H. Younan, S. Durba, and R. King, "Wavelet features for information mining in remote sensing archives," in *Geoscience and Remote Sensing Symposium, 2005. IGARSS'05. Proceedings. 2005 IEEE International*, vol. 8. IEEE, 2005, pp. 5630–5633.
- [41] V. P. Shah, N. H. Younan, S. S. Durbha, and R. L. King, "A systematic approach to wavelet-decomposition-level selection for image information mining from geospatial data archives," *IEEE Transactions on Geoscience and Remote Sensing*, vol. 45, no. 4, pp. 875–878, 2007.
- [42] Z. Shao, W. Zhou, L. Zhang, and J. Hou, "Improved color texture descriptors for remote sensing image retrieval," *journal of applied remote sensing*, vol. 8, no. 1, pp. 083 584–083 584, 2014.
- [43] S. Bouteldja and A. Kourgli, "Multiscale texture features for the retrieval of high resolution satellite images," in *Systems, Signals and Image Processing (IWSSIP), 2015 International Conference on*. IEEE, 2015, pp. 170–173.

- [44] G. B. Marchisio and J. Cornelison, "Content-based search and clustering of remote sensing imagery," in *Geoscience and Remote Sensing Symposium, 1999. IGARSS'99 Proceedings. IEEE 1999 International*, vol. 1. IEEE, 1999, pp. 290–292.
- [45] C. Li and V. Castelli, "Deriving texture feature set for content-based retrieval of satellite image database," in *Proceedings 1997 International Conference on Image Processing, ICIP '97, Santa Barbara, California, USA, October 26-29, 1997*, 1997, pp. 576–579.
- [46] K. Koperski and G. B. Marchisio, "Multi-level indexing and GIS enhanced learning for satellite imageries," in *Proceedings of the International Workshop on Multimedia Data Mining, MDM/KDD'2000, August 20th, 2000, Boston, MA, USA*, 2000, pp. 8–13.
- [47] J. Li and R. M. Narayanan, "Integrated spectral and spatial information mining in remote sensing imagery," *IEEE Trans. Geoscience and Remote Sensing*, vol. 42, no. 3, pp. 673–685, 2004.
- [48] S. D. Newsam and C. Kamath, "Retrieval using texture features in high-resolution multispectral satellite imagery," in *Defense and Security*. International Society for Optics and Photonics, 2004, pp. 21–32.
- [49] Y. Li and T. R. Bretschneider, "Semantics-based satellite image retrieval using low-level features," in *2004 IEEE International Geoscience and Remote Sensing Symposium, IGARSS 2004, Anchorage, Alaska, USA, 20-24 September 2004*, 2004, pp. 4406–4409.
- [50] P. Maheswary and N. Srivastava, "Retrieval of remote sensing images using colour and texture attribute," *CoRR*, vol. abs/0908.4074, 2009.
- [51] A. Samal, S. K. Bhatia, P. Vadlamani, and D. Marx, "Searching satellite imagery with integrated measures," *Pattern Recognition*, vol. 42, no. 11, pp. 2502–2513, 2009.
- [52] P. Maheshwary and N. Srivastava, "Prototype system for retrieval of remote sensing images based on color moment and gray level co-occurrence matrix," *P. Maheshwary and N. Srivastava, "Prototype System for Retrieval of Remote Sensing Images based on Color Moment and Gray Level Co-Occurrence Matrix", International Journal of Computer Science Issues, IJCSI, Volume 3, pp20-23, August 2009*, vol. 3, 2009.
- [53] Z. Shao, W. Zhou, and Q. Cheng, "Remote sensing image retrieval with combined features of salient region," *The International Archives of Photogrammetry, Remote Sensing and Spatial Information Sciences*, vol. 40, no. 6, p. 83, 2014.
- [54] H. Sebai, A. Kourgli, and A. Serir, "Dual-tree complex wavelet transform applied on color descriptors for remote-sensed images retrieval," *Journal of Applied Remote Sensing*, vol. 9, no. 1, pp. 095 994–095 994, 2015.
- [55] Q. Bao and P. Guo, "Comparative studies on similarity measures for remote sensing image retrieval," in *Proceedings of the IEEE International Conference on Systems, Man & Cybernetics: The Hague, Netherlands, 10-13 October 2004*, 2004, pp. 1112–1116.
- [56] L. Gueguen and M. Datcu, "A similarity metric for retrieval of compressed objects: Application for mining satellite image time series," *IEEE Transactions on Knowledge and Data Engineering*, vol. 20, no. 4, pp. 562–575, 2008.
- [57] M. Graña and M. A. Veganzones, "An endmember-based distance for content based hyperspectral image retrieval," *Pattern Recognition*, vol. 45, no. 9, pp. 3472–3489, 2012.
- [58] M. A. Veganzones, M. Datcu, and M. Grana, "Dictionary based hyperspectral image retrieval." in *ICPRAM (1)*, 2012, pp. 426–432.

- [59] M. Schröder, H. Rehrauer, K. Seidel, and M. Datcu, “Interactive learning and probabilistic retrieval in remote sensing image archives,” *IEEE Trans. Geoscience and Remote Sensing*, vol. 38, no. 5, pp. 2288–2298, 2000.
- [60] M. Ferecatu and N. Boujemaa, “Interactive remote-sensing image retrieval using active relevance feedback,” *IEEE Trans. Geoscience and Remote Sensing*, vol. 45, no. 4, pp. 818–826, 2007.
- [61] B. Demir and L. Bruzzone, “A novel active learning method in relevance feedback for content-based remote sensing image retrieval,” *IEEE Trans. Geoscience and Remote Sensing*, vol. 53, no. 5, pp. 2323–2334, 2015.
- [62] S. Aksoy, G. Marchisio, K. Koperski, and C. Tusk, “Probabilistic retrieval with a visual grammar,” in *Geoscience and Remote Sensing Symposium, 2002. IGARSS’02. 2002 IEEE International*, vol. 2. IEEE, 2002, pp. 1041–1043.
- [63] S. Aksoy, K. Koperski, C. Tusk, and G. Marchisio, “Interactive training of advanced classifiers for mining remote sensing image archives,” in *Proceedings of the tenth ACM SIGKDD international conference on Knowledge discovery and data mining*. ACM, 2004, pp. 773–782.
- [64] R. Datta, J. Li, A. Parulekar, and J. Z. Wang, “Scalable remotely sensed image mining using supervised learning and content-based retrieval,” *Pennsylvania State Univ., State College, PA, USA, Tech. Rep. CSE*, pp. 06–019, 2006.
- [65] M. Costache and M. Datcu, “Learning-unlearning for mining high resolution eo images,” in *Geoscience and Remote Sensing Symposium, 2007. IGARSS 2007. IEEE International*. IEEE, 2007, pp. 4761–4764.
- [66] Y. Li and T. R. Bretschneider, “Semantic-sensitive satellite image retrieval,” *IEEE Transactions on Geoscience and Remote Sensing*, vol. 45, no. 4, pp. 853–860, 2007.
- [67] A. S. Barb and C.-R. Shyu, “Visual information mining and ranking using graded relevance assessments in satellite image databases,” in *Geoscience and Remote Sensing Symposium (IGARSS), 2010 IEEE International*. IEEE, 2010, pp. 3398–3401.
- [68] A. S. Barb and C. Shyu, “Visual-semantic modeling in content-based geospatial information retrieval using associative mining techniques,” *IEEE Geosci. Remote Sensing Lett.*, vol. 7, no. 1, pp. 38–42, 2010.
- [69] E. Aptoula, “Remote sensing image retrieval with global morphological texture descriptors,” *IEEE Trans. Geoscience and Remote Sensing*, vol. 52, no. 5, pp. 3023–3034, 2014.
- [70] G. J. Scott, M. N. Klaric, C. H. Davis, and C. Shyu, “Entropy-balanced bitmap tree for shape-based object retrieval from large-scale satellite imagery databases,” *IEEE Trans. Geoscience and Remote Sensing*, vol. 49, no. 5, pp. 1603–1616, 2011.
- [71] J. Sivic and A. Zisserman, “Video google: A text retrieval approach to object matching in videos,” in *9th IEEE International Conference on Computer Vision (ICCV 2003), 14-17 October 2003, Nice, France, 2003*, pp. 1470–1477.
- [72] F. Perronnin and C. R. Dance, “Fisher kernels on visual vocabularies for image categorization,” in *2007 IEEE Computer Society Conference on Computer Vision and Pattern Recognition (CVPR 2007), 18-23 June 2007, Minneapolis, Minnesota, USA, 2007*.
- [73] H. Jégou, M. Douze, C. Schmid, and P. Pérez, “Aggregating local descriptors into a compact image representation,” in *The Twenty-Third IEEE Conference on Computer Vision and Pattern Recognition, CVPR 2010, San Francisco, CA, USA, 13-18 June 2010, 2010*, pp. 3304–3311.

- [74] W. Zhou, S. Newsam, C. Li, and Z. Shao, "Learning low dimensional convolutional neural networks for high-resolution remote sensing image retrieval," *Remote Sensing*, vol. 9, no. 5, p. 489, 2017.
- [75] P. Napoletano, "Visual descriptors for content-based retrieval of remote sensing images," *CoRR*, vol. abs/1602.00970, 2016.
- [76] M. Quartulli and I. G. Olaizola, "A review of eo image information mining," *ISPRS Journal of Photogrammetry and Remote Sensing*, vol. 75, pp. 11–28, 2013.
- [77] M. Datcu, S. d'Elia, R. L. King, and L. Bruzzone, "Introduction to the special section on image information mining for earth observation data," *IEEE Transactions on Geoscience and Remote Sensing*, vol. 45, no. 4, pp. 795–798, 2007.
- [78] M. Datcu, R. L. King, and S. D'Elia, "Introduction to the special issue on image information mining: Pursuing automation of geospatial intelligence for environment and security," *IEEE Geoscience and Remote Sensing Letters*, vol. 7, no. 1, pp. 3–6, 2010.
- [79] W. Zhou, S. Newsam, C. Li, and Z. Shao, "Patternnet: A benchmark dataset for performance evaluation of remote sensing image retrieval," *arXiv preprint arXiv:1706.03424*, 2017.
- [80] D. Peijun, C. Yunhao, T. Hong, and F. Tao, "Study on content-based remote sensing image retrieval," in *Geoscience and Remote Sensing Symposium, 2005. IGARSS'05. Proceedings. 2005 IEEE International*, vol. 2. IEEE, 2005, pp. 4–pp.
- [81] R. M. Haralick, K. S. Shanmugam, and I. Dinstein, "Textural features for image classification," *IEEE Trans. Systems, Man, and Cybernetics*, vol. 3, no. 6, pp. 610–621, 1973.
- [82] S. Mallat, "A theory for multiresolution signal decomposition: The wavelet representation," *IEEE Trans. Pattern Anal. Mach. Intell.*, vol. 11, no. 7, pp. 674–693, 1989.
- [83] A. Boggess, F. J. Narcowich, D. L. Donoho, and P. L. Donoho, "A first course in wavelets with fourier analysis," *Physics Today*, vol. 55, no. 5, p. 63, 2002.
- [84] J. G. Daugman, "Complete discrete 2-d gabor transforms by neural networks for image analysis and compression," *IEEE Trans. Acoustics, Speech, and Signal Processing*, vol. 36, no. 7, pp. 1169–1179, 1988.
- [85] B. S. Manjunath and W. Ma, "Texture features for browsing and retrieval of image data," *IEEE Trans. Pattern Anal. Mach. Intell.*, vol. 18, no. 8, pp. 837–842, 1996.
- [86] M. Pietikäinen, T. Ojala, and Z. Xu, "Rotation-invariant texture classification using feature distributions," *Pattern Recognition*, vol. 33, no. 1, pp. 43–52, 2000.
- [87] Z. Gu, C. Duncan, E. Renshaw, M. Mugglestone, C. Cowan, and P. Grant, "Comparison of techniques for measuring cloud texture in remotely sensed satellite meteorological image data," in *IEE Proceedings F-Radar and Signal Processing*, vol. 136, no. 5. IET, 1989, pp. 236–248.
- [88] A. R. Rao, *A taxonomy for texture description and identification*. Springer Science & Business Media, 2012.
- [89] A. P. Pentland, "Fractal-based description of natural scenes," *IEEE transactions on pattern analysis and machine intelligence*, no. 6, pp. 661–674, 1984.
- [90] E. Aptoula, "Extending morphological covariance," *Pattern Recognition*, vol. 45, no. 12, pp. 4524–4535, 2012.

- [91] —, “Comparative study of moment based parameterization for morphological texture description,” *J. Visual Communication and Image Representation*, vol. 23, no. 8, pp. 1213–1224, 2012.
- [92] D. G. Lowe, “Distinctive image features from scale-invariant keypoints,” *International Journal of Computer Vision*, vol. 60, no. 2, pp. 91–110, 2004.
- [93] G.-S. Xia, W. Yang, J. Delon, Y. Gousseau, H. Sun, and H. Maître, “Structural high-resolution satellite image indexing,” in *ISPRS TC VII Symposium-100 Years ISPRS*, vol. 38, 2010, pp. 298–303.
- [94] G. Liu, G.-S. Xia, W. Yang, and L. Zhang, “Texture analysis by using shapes co-occurrence patterns,” in *International Conference on Pattern Recognition*, 2014, pp. 1–6.
- [95] G. S. Xia, G. Liu, X. Bai, and L. Zhang, “Texture characterization using shape co-occurrence patterns,” *IEEE Transactions on Image Processing*, vol. PP, no. 99, pp. 1–1, 2017.
- [96] V. Caselles, B. Coll, and J. Morel, “Topographic maps and local contrast changes in natural images,” *International Journal of Computer Vision*, vol. 33, no. 1, pp. 5–27, 1999.
- [97] G.-S. Xia, J. Delon, and Y. Gousseau, “Shape-based invariant texture indexing,” *International Journal of Computer Vision*, vol. 88, no. 3, pp. 382–403, 2010.
- [98] M. Wang and T. Song, “Remote sensing image retrieval by scene semantic matching,” *IEEE Trans. Geoscience and Remote Sensing*, vol. 51, no. 5-1, pp. 2874–2886, 2013.
- [99] J. Wang, W. Yang, and R. Acharya, “Color clustering techniques for color-content-based image retrieval from image databases,” in *Proceedings of the International Conference on Multimedia Computing and Systems, ICMCS 1997, Ottawa, Ontario, Canada, June 3-6, 1997*, 1997, pp. 442–449.
- [100] A. Mir, M. Hanmandlu, and S. Tandon, “Texture analysis of ct images,” *IEEE Engineering in Medicine and Biology Magazine*, vol. 14, no. 6, pp. 781–786, 1995.
- [101] C. Yao and S. Chen, “Retrieval of translated, rotated and scaled color textures,” *Pattern Recognition*, vol. 36, no. 4, pp. 913–929, 2003.
- [102] P. R. Bingham, J. R. Price, K. W. Tobin, and T. P. Karnowski, “Semiconductor sidewall shape estimation,” *J. Electronic Imaging*, vol. 13, no. 3, pp. 474–485, 2004.
- [103] A. K. Shackelford and C. H. Davis, “A hierarchical fuzzy classification approach for high-resolution multispectral data over urban areas,” *IEEE Trans. Geoscience and Remote Sensing*, vol. 41, no. 9, pp. 1920–1932, 2003.
- [104] M. Pesaresi and J. A. Benediktsson, “A new approach for the morphological segmentation of high-resolution satellite imagery,” *IEEE Trans. Geoscience and Remote Sensing*, vol. 39, no. 2, pp. 309–320, 2001.
- [105] J. Li, J. Z. Wang, and G. Wiederhold, “IRM: integrated region matching for image retrieval,” in *Proceedings of the 8th ACM International Conference on Multimedia 2000, Los Angeles, CA, USA, October 30 - November 3, 2000.*, 2000, pp. 147–156.
- [106] R. Zhang and Z. Zhang, “A clustering based approach to efficient image retrieval,” in *14th IEEE International Conference on Tools with Artificial Intelligence (ICTAI 2002), 4-6 November 2002, Washington, DC, USA*, 2002, pp. 339–346.
- [107] D. Quattrochi, N. Lam, H. Qiu, and W. Zhao, “Image characterization and modeling system (icams): a geographic information system for the characterization and modeling of multiscale remote sensing data,” *Scale in Remote Sensing and GIS*, pp. 295–307, 1997.

- [108] C. W. Emerson, S. Chinniah, N. S.-N. Lam, and D. A. Quattrochi, "A region quadtree-based framework for similarity searches of image databases," in *Proceedings of Geocomputation*, 2005.
- [109] Y. Yang and S. D. Newsam, "Geographic image retrieval using local invariant features," *IEEE Trans. Geoscience and Remote Sensing*, vol. 51, no. 2, pp. 818–832, 2013.
- [110] E. Aptoula, "Bag of morphological words for content-based geographical retrieval," in *12th International Workshop on Content-Based Multimedia Indexing, CBMI 2014, Klagenfurt, Austria, June 18-20, 2014*, 2014, pp. 1–5.
- [111] J. Yang, J. Liu, and Q. Dai, "An improved bag-of-words framework for remote sensing image retrieval in large-scale image databases," *International Journal of Digital Earth*, vol. 8, no. 4, pp. 273–292, 2015.
- [112] P. Bosilj, E. Aptoula, S. Lefèvre, and E. Kijak, "Retrieval of remote sensing images with pattern spectra descriptors," *ISPRS Int. J. Geo-Information*, vol. 5, no. 12, p. 228, 2016.
- [113] P. Maragos, "Pattern spectrum and multiscale shape representation," *IEEE Trans. Pattern Anal. Mach. Intell.*, vol. 11, no. 7, pp. 701–716, 1989.
- [114] S. Özkan, T. Ates, E. Tola, M. Soysal, and E. Esen, "Performance analysis of state-of-the-art representation methods for geographical image retrieval and categorization," *IEEE Geosci. Remote Sensing Lett.*, vol. 11, no. 11, pp. 1996–2000, 2014.
- [115] H. Jégou, M. Douze, and C. Schmid, "Product quantization for nearest neighbor search," *IEEE Trans. Pattern Anal. Mach. Intell.*, vol. 33, no. 1, pp. 117–128, 2011.
- [116] Y. Wang, L. Zhang, X. Tong, L. Zhang, Z. Zhang, H. Liu, X. Xing, and P. T. Mathiopoulos, "A three-layered graph-based learning approach for remote sensing image retrieval," *IEEE Trans. Geoscience and Remote Sensing*, vol. 54, no. 10, pp. 6020–6034, 2016.
- [117] A. Oliva and A. Torralba, "Modeling the shape of the scene: A holistic representation of the spatial envelope," *International Journal of Computer Vision*, vol. 42, no. 3, pp. 145–175, 2001.
- [118] J. Yang, K. Yu, Y. Gong, and T. S. Huang, "Linear spatial pyramid matching using sparse coding for image classification," in *2009 IEEE Computer Society Conference on Computer Vision and Pattern Recognition (CVPR 2009), 20-25 June 2009, Miami, Florida, USA*, 2009, pp. 1794–1801.
- [119] W. Zhou, Z. Shao, C. Diao, and Q. Cheng, "High-resolution remote-sensing imagery retrieval using sparse features by auto-encoder," *Remote Sensing Letters*, vol. 6, no. 10, pp. 775–783, 2015.
- [120] Y. Li, Y. Zhang, C. Tao, and H. Zhu, "Content-based high-resolution remote sensing image retrieval via unsupervised feature learning and collaborative affinity metric fusion," *Remote Sensing*, vol. 8, no. 9, p. 709, 2016.
- [121] Y. LeCun, L. Bottou, Y. Bengio, and P. Haffner, "Gradient-based learning applied to document recognition," *Proceedings of the IEEE*, vol. 86, no. 11, pp. 2278–2324, 1998.
- [122] A. Krizhevsky, I. Sutskever, and G. E. Hinton, "Imagenet classification with deep convolutional neural networks," in *Advances in neural information processing systems*, 2012, pp. 1097–1105.
- [123] O. Russakovsky, J. Deng, H. Su, J. Krause, S. Satheesh, S. Ma, Z. Huang, A. Karpathy, A. Khosla, M. Bernstein *et al.*, "Imagenet large scale visual recognition challenge," *International Journal of Computer Vision*, vol. 115, no. 3, pp. 211–252, 2015.

- [124] J. Ng, F. Yang, and L. Davis, "Exploiting local features from deep networks for image retrieval," in *Proceedings of the IEEE Conference on Computer Vision and Pattern Recognition Workshops*, 2015, pp. 53–61.
- [125] A. Mousavian and J. Kosecka, "Deep convolutional features for image based retrieval and scene categorization," *arXiv preprint arXiv:1509.06033*, 2015.
- [126] A. Babenko and V. Lempitsky, "Aggregating deep convolutional features for image retrieval," *arXiv preprint arXiv:1510.07493*, 2015.
- [127] Y. Kalantidis, C. Mellina, and S. Osindero, "Cross-dimensional weighting for aggregated deep convolutional features," *arXiv preprint arXiv:1512.04065*, 2015.
- [128] V. Chandrasekhar, J. Lin, O. Morère, H. Goh, and A. Veillard, "A practical guide to cnns and fisher vectors for image instance retrieval," *arXiv preprint arXiv:1508.02496*, 2015.
- [129] A. Babenko, A. Slesarev, A. Chigorin, and V. Lempitsky, "Neural codes for image retrieval," in *Computer Vision—ECCV 2014*. Springer, 2014, pp. 584–599.
- [130] T. Uricchio, M. Bertini, L. Seidenari, and A. Bimbo, "Fisher encoded convolutional bag-of-windows for efficient image retrieval and social image tagging," in *Proceedings of the IEEE International Conference on Computer Vision Workshops*, 2015, pp. 9–15.
- [131] A. Gordo, J. Almazán, J. Revaud, and D. Larlus, "Deep image retrieval: Learning global representations for image search," in *Computer Vision - ECCV 2016 - 14th European Conference, Amsterdam, The Netherlands, October 11-14, 2016, Proceedings, Part VI*, 2016, pp. 241–257.
- [132] Y. Jia, E. Shelhamer, J. Donahue, S. Karayev, J. Long, R. Girshick, S. Guadarrama, and T. Darrell, "Caffe: Convolutional architecture for fast feature embedding," in *Proceedings of the ACM International Conference on Multimedia*. ACM, 2014, pp. 675–678.
- [133] K. Chatfield, K. Simonyan, A. Vedaldi, and A. Zisserman, "Return of the devil in the details: Delving deep into convolutional nets," *arXiv preprint arXiv:1405.3531*, 2014.
- [134] K. Simonyan and A. Zisserman, "Very deep convolutional networks for large-scale image recognition," *arXiv preprint arXiv:1409.1556*, 2014.
- [135] F. Perronnin and C. R. Dance, "Fisher kernels on visual vocabularies for image categorization," in *2007 IEEE Computer Society Conference on Computer Vision and Pattern Recognition (CVPR 2007), 18-23 June 2007, Minneapolis, Minnesota, USA*, 2007.
- [136] G.-S. Xia, J. Hu, F. Hu, B. Shi, X. Bai, Y. Zhong, L. Zhang, and X. Lu, "Aid: A benchmark data set for performance evaluation of aerial scene classification," *IEEE Transactions on Geoscience and Remote Sensing*, 2017.
- [137] M. A. Vezanones and M. Graña, "Endmember extraction methods: A short review," in *Knowledge-Based Intelligent Information and Engineering Systems, 12th International Conference, KES 2008, Zagreb, Croatia, September 3-5, 2008, Proceedings, Part III*, 2008, pp. 400–407.
- [138] A. Makedonas, D. Besiris, G. Economou, and S. Fotopoulos, "Dictionary based color image retrieval," *J. Visual Communication and Image Representation*, vol. 19, no. 7, pp. 464–470, 2008.
- [139] D. Cerra and M. Datcu, "Image retrieval using compression-based techniques," in *Source and Channel Coding (SCC), 2010 International ITG Conference on*. IEEE, 2010, pp. 1–6.

- [140] M. Li, X. Chen, X. Li, B. Ma, and P. M. B. Vitányi, “The similarity metric,” *IEEE Trans. Information Theory*, vol. 50, no. 12, pp. 3250–3264, 2004.
- [141] L. Si, R. Jin, S. C. H. Hoi, and M. R. Lyu, “Collaborative image retrieval via regularized metric learning,” *Multimedia Syst.*, vol. 12, no. 1, pp. 34–44, 2006.
- [142] S. C. H. Hoi, W. Liu, and S. Chang, “Semi-supervised distance metric learning for collaborative image retrieval and clustering,” *TOMCCAP*, vol. 6, no. 3, pp. 18:1–18:26, 2010.
- [143] C. Huang, S. Zhu, and K. Yu, “Large scale strongly supervised ensemble metric learning, with applications to face verification and retrieval,” *CoRR*, vol. abs/1212.6094, 2012.
- [144] J. Lee, R. Jin, and A. K. Jain, “Rank-based distance metric learning: An application to image retrieval,” in *2008 IEEE Computer Society Conference on Computer Vision and Pattern Recognition (CVPR 2008)*, 24–26 June 2008, Anchorage, Alaska, USA, 2008.
- [145] B. Chaudhuri, B. Demir, L. Bruzzone, and S. Chaudhuri, “Region-based retrieval of remote sensing images using an unsupervised graph-theoretic approach,” *IEEE Geoscience and Remote Sensing Letters*, vol. 13, no. 7, pp. 987–991, 2016.
- [146] R. Arandjelovic, P. Gronát, A. Torii, T. Pajdla, and J. Sivic, “Netvlad: CNN architecture for weakly supervised place recognition,” in *2016 IEEE Conference on Computer Vision and Pattern Recognition, CVPR 2016, Las Vegas, NV, USA, June 27–30, 2016*, 2016, pp. 5297–5307.
- [147] R. A. Baeza-Yates and B. A. Ribeiro-Neto, *Modern Information Retrieval*. ACM Press / Addison-Wesley, 1999.
- [148] A. Rakotomamonjy, F. R. Bach, S. Canu, and Y. Grandvalet, “Simplemkl,” *Journal of Machine Learning Research*, vol. 9, no. Nov, pp. 2491–2521, 2008.
- [149] C. Buckley and G. Salton, “Optimization of relevance feedback weights,” in *SIGIR’95, Proceedings of the 18th Annual International ACM SIGIR Conference on Research and Development in Information Retrieval. Seattle, Washington, USA, July 9–13, 1995 (Special Issue of the SIGIR Forum)*, 1995, pp. 351–357.
- [150] Y. Ishikawa, R. Subramanya, and C. Faloutsos, “Mindreader: Querying databases through multiple examples,” in *VLDB’98, Proceedings of 24rd International Conference on Very Large Data Bases, August 24–27, 1998, New York City, New York, USA, 1998*, pp. 218–227.
- [151] I. J. Cox, M. L. Miller, S. M. Omohundro, and P. N. Yianilos, “Pichunter: Bayesian relevance feedback for image retrieval,” in *13th International Conference on Pattern Recognition, ICPR 1996, Vienna, Austria, 25–19 August, 1996*, 1996, pp. 361–369.
- [152] I. J. Cox, M. L. Miller, T. P. Minka, T. V. Papatthomas, and P. N. Yianilos, “The bayesian image retrieval system, pichunter: theory, implementation, and psychophysical experiments,” *IEEE Trans. Image Processing*, vol. 9, no. 1, pp. 20–37, 2000.
- [153] S. Tong and E. Y. Chang, “Support vector machine active learning for image retrieval,” in *Proceedings of the 9th ACM International Conference on Multimedia 2001, Ottawa, Ontario, Canada, September 30 - October 5, 2001*, 2001, pp. 107–118.
- [154] L. Zhang, F. Lin, and B. Zhang, “A neural network based self-learning algorithm of image retrieval,” *Chinese Journal of Software*, vol. 12, no. 10, pp. 1479–1485, 2001.
- [155] L. Mascolo, M. Quartulli, P. Guccione, G. Nico, and I. G. Olaizola, “Distributed mining of large scale remote sensing image archives on public computing infrastructures,” *CoRR*, vol. abs/1501.05286, 2015.

- [156] N. Ramesh and I. Sethi, “A model based industrial part recognition system using hashing,” in *Proc. 22nd Intl. Symposium on Industrial Robots, Intl. Robots and Vision Automation Conf*, 1991, pp. 37–51.
- [157] I. K. Sethi and N. Ramesh, “Local association based recognition of two-dimensional objects,” *Mach. Vis. Appl.*, vol. 5, no. 4, pp. 265–276, 1992.
- [158] B. Demir and L. Bruzzo, “Kernel-based hashing for content-based image retrval in large remote sensing data archive,” in *Geoscience and Remote Sensing Symposium (IGARSS), 2014 IEEE International*. IEEE, 2014, pp. 3542–3545.
- [159] B. Demir and L. Bruzzzone, “Hashing-based scalable remote sensing image search and retrieval in large archives,” *IEEE Trans. Geoscience and Remote Sensing*, vol. 54, no. 2, pp. 892–904, 2016.
- [160] C. Szegedy, W. Liu, Y. Jia, P. Sermanet, S. Reed, D. Anguelov, D. Erhan, V. Vanhoucke, and A. Rabinovich, “Going deeper with convolutions,” in *Proceedings of the IEEE Conference on Computer Vision and Pattern Recognition*, 2015, pp. 1–9.
- [161] F. Perronnin, J. Sánchez, and T. Mensink, “Improving the fisher kernel for large-scale image classification,” in *Computer Vision–ECCV 2010*. Springer, 2010, pp. 143–156.
- [162] Q. Zou, L. Ni, T. Zhang, and Q. Wang, “Deep learning based feature selection for remote sensing scene classification,” *Geoscience and Remote Sensing Letters, IEEE*, vol. 12, no. 11, pp. 2321–2325, 2015.
- [163] Y. Yang and S. Newsam, “Bag-of-visual-words and spatial extensions for land-use classification,” in *Proceedings of the 18th SIGSPATIAL International Conference on Advances in Geographic Information Systems*. ACM, 2010, pp. 270–279.
- [164] B. S. Manjunath, J.-R. Ohm, V. V. Vasudevan, and A. Yamada, “Color and texture descriptors,” *Circuits and Systems for Video Technology, IEEE Transactions on*, vol. 11, no. 6, pp. 703–715, 2001.
- [165] T. Deselaers, D. Keysers, and H. Ney, “Features for image retrieval: an experimental comparison,” *Information Retrieval*, vol. 11, no. 2, pp. 77–107, 2008.